Global profiling of lncRNAs-miRNAs-mRNAs reveals differential expression of coding genes and non-coding RNAs in the lung of Beagle dogs at different stages of *Toxocara canis* infection

Wen-Bin Zheng [a,b,1], Yang Zou [a,1], Jun-Jun He [a,*], Hany M. Elsheikha [c], Guo-Hua Liu [b], Min-Hua Hu [d], Shui-Lian Wang [b], Xing-Quan Zhu [a,e,*]

[a] *State Key Laboratory of Veterinary Etiological Biology, Key Laboratory of Veterinary Parasitology of Gansu Province, Lanzhou Veterinary Research Institute, Chinese Academy of Agricultural Sciences, Lanzhou, Gansu Province 730046, China*

[b] *Hunan Provincial Key Laboratory of Protein Engineering in Animal Vaccines, College of Veterinary Medicine, Hunan Agricultural University, Changsha, Hunan Province 410128, China*

[c] *Faculty of Medicine and Health Sciences, School of Veterinary Medicine and Science, University of Nottingham, Sutton Bonington Campus, Loughborough, LE12 5RD, UK*

[d] *National Canine Laboratory Animal Resource Center, Guangzhou General Pharmaceutical Research Institute Co., Ltd, Guangzhou, Guangdong Province 510240, China*

[e] *College of Veterinary Medicine, Shanxi Agricultural University, Taigu, Shanxi Province 030801, China*

* Corresponding author. State Key Laboratory of Veterinary Etiological Biology, Key Laboratory of Veterinary Parasitology of Gansu Province, Lanzhou Veterinary Research Institute, Chinese Academy of Agricultural Sciences, Lanzhou, Gansu Province 730046, China

E-mail addresses: hejunjun@caas.cn (J.J. He); xingquanzhu1@hotmail.com (X.Q. Zhu)

[1]These authors contributed equally

ABSTRACT

The roundworm *Toxocara canis* causes toxocariasis in dogs and larval migrans in humans. Better understanding of the lung response to *T. canis* infection could explain why *T. canis*

must migrate to and undergoes part of its development inside the lung of the definitive host. In this study, we profiled the expression patterns of long non-coding RNAs (lncRNAs), microRNAs (miRNAs), and mRNAs in the lungs of Beagle dogs infected by *T. canis*, using high throughput RNA sequencing. At 24 h p.i., 1,012 lncRNAs, 393 mRNAs and 10 miRNAs were differentially expressed (DE). We also identified 883 DElncRNAs, 264 DEmRNAs and 20 DEmiRNAs at 96 h p.i., and 996 DElncRNAs, 342 DEmRNAs and eight DEmiRNAs at 36 days p.i., between infected and control dogs. Significant changes in the levels of expression of transcripts related to immune response and inflammation were associated with the antiparasitic response of the lung to *T. canis*. The remarkable increase in the expression of *scgb1a1* at all time points after infection suggests the need for consistent moderation of the excessive inflammatory response. Also, upregulation of *foxj1* at 24 h p.i., and downregulation of *IL-1β* and *IL-21* at 96 h p.i., suggest an attenuation of the humoral immunity of infected dogs. These results indicate that *T. canis* pathogenesis in the lung is mediated through contributions from both pro-inflammatory and anti-inflammatory mechanisms. Competing endogenous RNA (ceRNA) network analysis revealed significant interactions between DElncRNAs, DEmiRNAs and DEmRNAs, and improved our understanding of the ceRNA regulatory mechanisms in the context of *T. canis* infection. These data provide comprehensive understanding of the regulatory networks that govern the lung response to *T. canis* infection and reveal new mechanistic insights into the interaction during the course of *T. canis* infection of canine lung in both the host and the parasite.

Keywords:
Toxocariasis
Toxocara canis
Transcriptomics
Beagle dog
Lung

1. Introduction

The ascarid roundworm *Toxocara canis* infects the small intestine of dogs and can be transmitted to other mammals including humans (Ma et al., 2018). This parasite is highly zoonotic and has been listed as one of the five neglected parasitic infections by the American Centers for Disease Control and Prevention (https://www.cdc.gov/parasites/npi/). *Toxocara canis* is widespread throughout the world and environmental contamination with *T. canis* eggs is very common in soil samples, especially in urban public parks (Chen et al., 2018; Fakhri et al., 2018). *Toxocara canis* has a complex life cycle and during its development the parasite encounters diverse and multiple physiological niches inside the host (Maizels, 2013). Following ingestion of infectious eggs by the canine definitive host, larvae are released from eggs in the intestine where they penetrate the intestinal wall and migrate to the liver, heart and lung. Larvae penetrate through the alveolar wall and migrate up to the trachea and pharynx, where they are swallowed and enter the intestine to complete their development into adult worms.

In the paratenic and accidental hosts, the pulmonary phase of the life cycle is missing; larvae migrate through the blood vessel and spread to various tissues where they become arrested at the L3 stage for extensive periods without reaching the trachea, which is a prerequisite route to re-enter the host digestive tract (Webster, 1958). This dichotomy in the parasite's behavior between the natural host and paratenic/accidental host raised an interesting question as to why *T. canis* requires a lung migratory phase during its development inside the definitive host, particularly if the parasite takes up residence in the definitive host's intestine. Also, what role does the lung play during the pulmonary component of the *T. canis* lifecycle? (Craig and Scott, 2014). Impaired lung function due to *T. canis* infection manifests as coughing, eosinophilic pneumonia and asthma, and the severity of the respiratory manifestations correlates with the larval load in the lung (Kuzucu, 2006). Therefore, in this strategic anatomical location, lung tissues must play an eminent role in host defense by recognizing and responding to *T. canis* invasion. On the other hand, *T. canis* has to deal with the lung defense mechanisms to ensure its own survival. The outcome of this host-parasite interaction determines the outcome of infection. How *T. canis* maintains its survival under these hostile circumstances is largely unknown.

Previous studies involving high-throughput genomic, transcriptomic and proteomic approaches have been performed in order to explore the systems biology of *T. canis* (Zhu et al., 2015; Zheng et al., 2020). Also, metabolomics showed that *T. canis* infection can alter

some important metabolic pathways in the definitive host (Zheng et al., 2019). Additionally, microarray analysis revealed transcriptional differences in neurotoxocarosis caused by *T. canis* and *Toxocara cati* (Janecek et al., 2015). Despites these efforts, genomic information regarding the interaction between *T. canis* and the complex microenvironment of the host lung is lacking. Similarly, we do not have a detailed understanding of the extent of transcriptional regulation during lung infection, including temporal changes in expression of long non-coding RNAs (lncRNAs), microRNAs (miRNAs) and mRNAs, and changes in transcription factors (TFs). These different types of regulatory information need to be simultaneously collected in order to reconstruct an accurate and detailed understanding of the canine lung response to *T. canis* infection.

In the present study, we investigated alterations in the expression of lncRNAs, miRNAs and mRNAs in the lungs of Beagle dogs infected by *T. canis*, at different stages of infection. Our data provided comprehensive information about *T. canis* infection-related gene expression trajectories and key regulators of specific immunological mechanisms that mediate the interaction between *T. canis* and the canine lung.

2. Materials and methods

2.1. Ethics statement

The study was approved by the Animal Administration and Ethics Committee of Lanzhou Veterinary Research Institute, Chinese Academy of Agricultural Sciences, People's Republic of China (Approval no. 2018-015). The dogs used in the study were handled in accordance with the laboratory animal-microbiological standards and monitoring (Standard id: GB 14922.2-2011). Good animal husbandry and welfare practices were followed as stipulated by the Animal Ethics Procedures and Guidelines of the People's Republic of China.

2.2. Animal infection and lung sample collection

Six to 7 weeks old Beagle puppies (n = 18) were purchased from, and housed at, the National Canine Laboratory Animal Resource Center, China. To ensure that each puppy was sero-negative for *T. canis* infection, anti-*T. canis* IgG antibodies were examined in the sera of the puppies by an indirect ELISA using larval excretory-secretory antigen as previously described (Regis et al., 2011). Also, feces from all puppies were examined by the sugar flotation method to ensure each puppy was free of gastrointestinal parasites. Puppies were

randomly assigned to three infected and three matched uninfected (control) groups. Each group included three biological replicates. Eggs of *T. canis* were collected from the uteri of fertile *T. canis* females. The eggs were incubated on filter papers with 0.5% formalin solution at 28 °C with 85–95% relative humidity for 4 weeks. The infectious eggs were collected from the filter papers and filtered using 200 mesh screens, then stored in 1% formalin solution at 4 °C (Zheng et al., 2019). Puppies in the infected group were inoculated orally with 300 infectious *T. canis* eggs in 1 ml of sterile isotonic saline, while puppies in the control groups were mock infected with saline only. At 24 h, 96 h and 36 days p.i., lung samples were collected and stored in liquid nitrogen until used for RNA extraction. The number of blood eosinophils was determined at the three time points p.i. by an automatic blood analyzer (XT2000 iv; Sysmex, Kobe, Japan). A student's *t*-test was used to assess the significance of difference in the level of eosinophilia between infected and control puppies. To recover *T. canis* larvae, a half-lung of each puppy was shredded and incubated for 12 h at 37 ºC with 1% mycillin and *T. canis* larvae were isolated by using a modified Baermann apparatus (Takamiya and Mita, 2016). The internal transcribed spacer (ITS) region of *T. canis* was amplified by PCR (Mikaeili et al., 2017) and sequenced by Sangon Biotech (Shanghai, China) to confirm mono-infection by *T. canis*.

2.3. Total RNA extraction and quality control

The total RNA was extracted from frozen lung tissue using TRIZOL (Life Technologies, Carlsbad, USA). Genomic DNA was removed from total RNA using DNase I (NEB, Ipswich, USA). The concentration and integrity of the extracted RNA were evaluated using a Qubit® 2.0 Flurometer (Life Technologies, Carlsbad, USA) and an Agilent Bioanalyzer 2100 system (Agilent Technologies, Santa Clara, USA), respectively. High quality samples with a high RNA integrity number (RIN) value > 8.0 were used to construct the sequencing libraries.

2.4. Library preparation for lncRNA sequencing

A total amount of 20 ng of RNA per sample was used as input material for the RNA sample preparation. LncRNAs and mRNAs were enriched by depleting the rRNAs from the total RNA by using the Epicentre Ribo-zero™ rRNA Removal Kit (Madison, WI, USA), and rRNA-free residue was cleaned up by ethanol precipitation. Then, 18 lncRNA libraries (one/puppy) were constructed using the rRNA-depleted RNA and a NEBNext® Ultra™ Directional RNA Library Prep Kit for Illumina® (NEB, Ipswich, USA), following the

manufacturer's recommendations. The fragmentation was performed using divalent cations under elevated temperature in NEBNext First Strand Synthesis Reaction Buffer (5X). First strand cDNA was synthesized using a random hexamer primer and M-MuLV Reverse Transcriptase (RNase H-). Second strand cDNA synthesis was subsequently performed using DNA Polymerase I and RNase H. In the reaction buffer, dNTPs with dTTP were replaced by dUTP. Remaining overhangs were converted into blunt ends via exonuclease/polymerase activities. After adenylation of the 3' ends of DNA fragments, a NEBNext Adaptor with hairpin loop structure were ligated for hybridization. In order to select cDNA fragments of preferentially ~150 to 200 bp in length, the library fragments were purified with an AMPure XP system (Beckman Coulter, Beverly, USA). Then, 3 μL of USER Enzyme (NEB, Ipswich, USA) was used with size-selected, adaptor-ligated cDNA at 37 ºC for 15 min followed by 5 min at 95 ºC before PCR amplification. Then, PCR was performed with Phusion High-Fidelity DNA polymerase (NEB, Ipswich, USA), Universal PCR primers and Index (X) Primer. The final products were purified on the AMPure XP system and the library quality was assessed on the Agilent Bioanalyzer 2100 system (Zhou et al., 2017).

2.5. Library preparation for small RNA sequencing

Eighteen small RNA libraries were constructed using a NEBNext® Multiplex Small RNA Library Prep Set for Illumina® (NEB, Ipswich, USA.) as previously described (Zhou et al., 2017). Index codes were added to attribute sequences to the corresponding samples, and cDNA fragments of 140 to 160 bp were recovered and dissolved in 8 μl of elution buffer (Zhou et al., 2017). Then, the quality of libraries was assessed using an Agilent Bioanalyzer 2100 system.

2.6. Clustering and sequencing

The clustering of the index-coded samples was performed on a cBot Cluster Generation System (Illumia, San Diego, USA) using a TruSeq PE Cluster Kit v3-cBot-HS (Illumia) according to the manufacturer's instructions. After cluster generation, the libraries were sequenced on the Illumina Nova_X platform, and 150 bp paired-end reads were generated for lncRNA libraries and 50 bp single-end reads were generated for small RNA libraries (Zhang et al., 2019).

2.7. Identification of lncRNA and mRNA

The original raw data in fastq format were processed using in-house Perl and Python

scripts. Clean reads were obtained by removing reads with poly-N, adapters, insert tags and low quality reads (He et al., 2017). Then, we calculated the Q20 (base ratio > 20), Q30 (base ratio > 30) and GC content of the clean data. The clean data were mapped to the reference genome of *Canis lupus familiaris* with HISAT2 (v2.0.4) (Langmead and Salzberg, 2012). Genome and annotation files of *Canis lupus familiaris* were downloaded from the Ensembl database (CanFam3.1). The mapped reads were assembled by StringTie (v1.3.3) (Pertea et al., 2016). Q20 > 95% and Q30 > 85% were set as indicators of the good quality of the dataset. Known protein-coding genes were determined by HTSeq (Anders et al., 2015). lncRNA transcripts were screened with exon $\geqslant$ 2, fragments per kilobase of exon model per million reads mapped (FPKM) $\geqslant$ 0.5 and length > 200 bp. lncRNAs that overlap with the exon area in the reference annotation file were considered as known lncRNAs. Then, the remaining transcripts were further filtered to identify their protein-coding potential. All transcripts with a coding-noncoding index (CNCI) score > 0, CPC2 coding probability > 0.5 or for which Pfam-scan tool search yielded even one protein domain hit were excluded (Punta et al., 2012; Sun et al., 2013; Kang et al., 2017), and the remaining transcripts without any coding potential were considered novel lncRNAs.

2.8. Identification of miRNA

Clean reads were obtained by removing low quality reads, 3' spliced reads, 5' joint contaminated reads, and reads with a length of less than 18 nucleotides (nt) or with poly-A from the original data. Then, the clean reads with ~18 to 35 nt were mapped to the reference genome using Bowtie (Langmead et al., 2009). Mapped small RNA tags were used to search for known miRNA. MiRbase 20.0 was used as a reference, and the modified software miRdeep 2 (Friedlander et al., 2012) and srna-tools-cli (Moxon et al., 2008) were used to identify the potential miRNAs and draw the secondary structures. In-house scripts were used to obtain the miRNA counts and the base bias on the first position of the identified miRNA with a certain length and on each position of all identified miRNA. To remove tags originating from protein-coding genes, repeat sequences, rRNA, tRNA, small nuclear RNA, and small nucleolar RNA, miRNA tags were mapped to the Rfam database or data for the specified species. The characteristics of hairpin structure of the miRNA precursor can be used to predict novel miRNAs. The software miREvo (Wen et al., 2012) and miRdeep 2 (Friedlander et al., 2012) were combined to predict novel miRNAs through exploring the secondary structure, the Dicer cleavage site and the minimum free energy of the small RNA tags unannotated in the

former steps. Also, custom scripts were used to obtain the identified miRNA counts and the base bias on the first position with a certain length and on each position of all identified miRNAs, respectively.

2.9. Identification of differentialy expressed lncRNAs, mRNAs and miRNAs

The expression levels of lncRNAs and mRNAs were determined by FPKM (Pertea et al., 2016), and miRNAs were analyzed by Transcripts Per Million (TPM) reads (Zhou et al., 2010). Differential expression between infected and control groups was assessed using DESeq2 software (Love et al., 2014). P values < 0.05 and absolute fold-change values > 1 was set as the thresholds for the differential expression of lncRNAs, mRNAs and miRNAs. In addition, Venn diagrams were used to visualize the overall distribution of differentially expressed (DE) lncRNAs, mRNAs and miRNAs.

2.10. Target gene prediction, and gene ontology and enrichment analysis

Because lncRNA can regulate the expression of adjacent genes, the *cis* target genes within 100 kb upstream and downstream of the lncRNA were analyzed and used to predict the lncRNA function. The GOseq R package (Young et al., 2010) was used for Gene Ontology (GO) enrichment analysis of the DElncRNAs and DEmRNAs. GO terms, including biological process (BP), cellular component (CC), and molecular function (MF), with $P < 0.05$ were considered significantly enriched. To identify the over-represented *T. canis* infection response signaling pathways, we performed Kyoto Encyclopedia of Genes and Genomes (KEGG) pathway enrichment analysis via a web server for annotation and enrichment analysis, KOBAS 3.0 (Wu et al., 2006). Gene pathway analysis of significant DEmRNAs was carried out with $P < 0.05$.

2.11. Construction of ceRNA networks of lncRNA-miRNA-mRNA

Target mRNAs and lncRNAs of miRNAs were predicted by miRanDa (Enright et al., 2003). The potential target relationship of DEmiRNA-DEmRNA and DEmiRNA-DElncRNA were analyzed based on the differentially expressed transcripts at 24 h p.i., 96 h p.i. and 36 days p.i., respectively. Then, all DEmRNAs and DElncRNAs regulated by the same DEmiRNAs were screened based on potential target relationships. Finally, the regulatory ceRNA networks of interacting DElncRNAs-DEmiRNAs-DEmRNAs at 24 h p.i., 96 h p.i. and 36 days p.i. were constructed and visualized using Cytoscape v.3.5 (Lotia et al., 2013).

2.12. Experimental validation using qRT-PCR

We selected five DEmRNAs, three DElncRNAs and 10 DEmiRNAs for the validation of RNA-Seq results by quantitative real-time PCR (qRT-PCR). A PrimeScript™ RT reagent Kit with gDNA (genomic DNA) Eraser (Takara, Tokyo, Japan), a lnRcute lncRNA cDNA first chain synthesis Kit (TianGen, Beijing, China) and a miRcute enhanced miRNA cDNA first chain synthesis Kit (TianGen, Beijing China) were used to synthesize the first strand cDNA of mRNA, lncRNA and miRNA, respectively. An EvaGreen qPCR MasterMix-no dye qRT-PCR Kit (abm, Zhenjiang, China), a lnRcute lncRNA qRT-PCR Kit (TianGen, Beijing, China) and a miRcute enhanced miRNA qRT-PCR Kit (TianGen, Beijing, China) were used for amplification of mRNAs, lncRNAs and miRNAs, respectively. The qRT-PCRs were run in triplicate on a LightCycler480 (Roche, Basel, Switzerland). mRNA amplification conditions were 95 °C for 10 min, 40 cycles of 94 °C for 15 s, 60 °C for 1 min. lncRNA amplification included the following conditions: 95 °C for 3 min, 40 cycles of 94 °C for 5 s, 60 °C for 15 s. miRNA amplification conditions included 95 °C for 15 min, 40 cycles of 94 °C for 20 s, 60 °C for 34 s. Melting curve analysis was performed to ensure specific amplification in each reaction, using the following conditions: 95 °C for 10 s, 65 °C for 1 min and a progressive increase from 65 °C to 95 °C. The expression levels of the selected DEmRNAs, DElncRNAs and DEmiRNAs were normalized to those of the house-keeping genes. All genes and primers are shown in Table 1.

3. Results

3.1. Identification of T. canis infection in dogs

Dogs used in the study were free of *T. canis* or any other gastrointestinal helminthic infection prior to the experiment. Although no severe clinical signs, such as cough or dyspnea, were observed in infected dogs, eosinophilia was found to increase over the course of infection. However, the difference in blood eosinophil counts at all time points between *T. canis*-infected and control dogs was not statistically significant (Fig. 1). At 96 h p.i., *T. canis* larvae were found in the lungs of all infected puppies with an average of 27.3 *T. canis* larvae per lung. At 36 days p.i., *T. canis* were found in the small intestines of all puppies in infected groups with an average of 75.3 *T. canis* per puppy. Also, anti-*T. canis* IgG antibodies were detected at 36 days p.i. in infected dogs. As expected, no *T. canis* was found in any puppy of the control groups. The partial sequence of ITS 1 and ITS 2 of infectious eggs, larvae and

adult worms recovered from infected puppies had 99.70% and 99.11% homology to the published sequences (GenBank accession no. **JF837169.1**), respectively, confirming mono-infection with *T. canis* in infected puppies.

3.2. Characteristic features of RNA-sequencing data

In lncRNA libraries, 2,299,561,678 raw reads, including 2,255,459,896 clean reads and 338.33 Gb of clean data were obtained, with an average of 18.80 Gb clean data per sample. The Q20 and Q30 of the raw reads were 95.77% and 89.40%, respectively, showing that the data were of good quality. Also, 92.08% clean reads were mapped to the *Canis lupus familiaris* reference genome. In small RNA libraries, 244,580,956 raw reads, including 238,913,114 clean reads and 12.23 Gb of clean data were produced, with an average of 0.67 Gb of clean data per sample. The Q20 and Q30 averages of raw reads were 99.82% and 99.52%, respectively. Additionally, 92.98% of the clean reads with ~18 to 35 bp length were successfully mapped to the reference genome. These results showed the good quality of both lncRNA and small RNA libraries. In this study, a total of 1,570 annotated lncRNA transcripts, 25,157 mRNA transcripts and 306 known miRNA transcripts, as well as 20,760 novel lncRNA transcripts and 151 novel miRNA transcripts, were identified. The workflow of data processing and the associated outputs are shown in Fig. 2. The raw data for RNA-seq analysis have been submitted to the NCBI Sequence Read Archive (SRA) under accession number **PRJNA577160**.

3.3. Differential expression of lncRNA, mRNA and miRNA

Here, we identified the regulatory networks of lncRNAs, mRNAs, and miRNAs in infected lung samples by analyzing the DElncRNAs, DEmRNAs, and DEmiRNAs. As shown in Fig. 3A-D and Supplementary Table S1, 1,012 DElncRNAs, 393 DEmRNAs and 10 DEmiRNAs were identified between infected and control dogs at 24 h p.i.. At 96 h p.i., 883 DElncRNAs, 264 DEmRNAs and 20 DEmiRNAs were identified between infected and control dogs. At 36 days p.i., 996 DElncRNAs, 342 DEmRNAs and eight DEmiRNAs were identified between infected and control dogs. Also, 56 DElncRNAs, 18 DEmRNAs and one DEmiRNA were common at all three time points after infection. The RNA-seq results were validated with five DEmRNAs (Fig. 4A-E), three DElncRNAs (Fig. 4F-H) and 10 DEmiRNAs using qRT-PCR analysis (Fig. 4I). The qRT-PCR verification demonstrated an overall similarity in the direction and magnitude of the expression measured by RNA sequencing and qRT-PCR.

3.4. Target gene prediction and function analysis of lncRNA

In this study, 22,677 transcripts of mRNA were identified within 100 kb upstream and downstream of the annotated and novel lncRNA. Among these, at 24 h p.i., 52 DEmRNAs were located within the upstream or downstream of 60 DElncRNAs. At 96 h p.i., 46 DEmRNAs were found in the adjacent area of 55 DElncRNAs. At 36 days p.i., 60 DEmRNAs were found within the upstream or downstream of 66 DElncRNAs (Supplementary Fig. S1 and Supplementary Table S2). These DElncRNAs may be involved in the interaction between *T. canis* and the lung by regulating expression of the adjacent mRNAs.

GO and KEGG enrichment analyses were performed using the predicted target genes of DElncRNAs. Enrichment results showed that 528 and 516 GO terms were significantly enriched at 24 h p.i. and 96 h p.i., and 505 GO terms were significantly enriched at 36 days p.i. (Supplementary Table S3). Also, 20 pathways were significantly enriched at 24 h p.i., including systemic lupus erythematosus, asthma and tuberculosis; 10 pathways were significantly enriched at 96 h p.i., including hematopoietic cell lineage, basal transcription factors and asthma; and five pathways were significantly enriched at 36 days p.i., including RNA transport, legionellosis, ribosome, hematopoietic cell lineage and sulfur metabolism (Supplementary Fig. S2 and Supplementary Table S4).

At 24 h p.i., 295 predicted target genes (e.g. *oasl*, *ubqln1* and *sox4*) of DElncRNAs (including 267 DElncRNAs) were significantly enriched in 66 immune- or inflammation-related GO terms. At 96 h p.i. 266 predicted target genes (e.g. *IL-21*, *bpifb1* and *runx1*) of DElncRNAs (including 236 DElncRNAs), were significantly enriched in 77 immune- or inflammation-related GO terms. At 36 days p.i., 327 predicted target genes (e.g. *bpifa1*, *gpnmb* and *slpi*) of DElncRNAs (including 297 DElncRNAs) were significantly enriched in 75 immune- or inflammation-related GO terms (Supplementary Table S5). The top 30 immune- or inflammation-related differential GO terms are shown in Supplementary Fig. S3.

3.5. GO and KEGG pathway analysis of differentially expressed mRNAs

At 24 h p.i., 312 DEmRNAs were significantly enriched in 423 GO terms; at 96 h p.i., 218 DEmRNAs were significantly enriched in 479 GO terms; and at 36 days p.i., 268 DEmRNAs were significantly enriched in 585 GO terms (Supplementary Table S6). The top 30 differential GO terms are shown in Supplementary Fig. S4. Regarding KEGG enrichment analysis at 24 h p.i., 39 DEmRNAs were significantly enriched in 10 pathways such as

legionellosis, pancreatic secretion and phagosome. At 96 h p.i., 19 DEmRNAs were significantly enriched in 12 pathways, for example pancreatic secretion, glutamatergic synapse and inflammatory mediator regulation of transient receptor potentical (TRP) channels. And at 36 days p.i., 41 DEmRNAs were significantly enriched in 10 pathways such as cytokine-cytokine receptor interaction, Jak-STAT signaling pathway and systemic lupus erythematosus (Supplementary Table S7). The top 20 most highly represented pathways in each group are shown in Fig. 5. A total of 101 common signaling pathways were found at 24 h p.i., 96 h p.i. and 36 days p.i. The common pathways with DEmRNAs $\geqslant$ 3 during *T. canis* infection are listed in Table 2. The largest numbers of enriched DEmRNAs were found in metabolic pathways and cytokine-cytokine receptor interaction pathway.

We also identified the immune- or inflammation-related GO terms of the key DEmRNAs that participate in *T. canis* infection (Supplementary Table S8). At 24 h p.i., 19 DEmRNAs were significantly enriched in 34 immune- or inflammation-related GO terms, including 11 upregulated DEmRNAs and eight downregulated DEmRNAs. At 96 h p.i., 44 DEmRNAs were significantly enriched in 124 immune- or inflammation-related GO terms, including 20 upregulated DEmRNAs and 24 downregulated DEmRNAs. At 36 days p.i., 59 DEmRNAs were significantly enriched in 111 immune- or inflammation-related GO terms, including 40 upregulated DEmRNAs and 19 downregulated DEmRNAs. The top 30 immune- or inflammation-related differential GO terms are shown in Supplementary Fig. S5.

3.6. ceRNA networks of lncRNA-miRNA-mRNA

The ceRNA networks were constructed based on potential target relationships between DElncRNAs, DEmiRNAs, and DEmRNAs, and included 45 DElncRNAs, three DEmiRNAs and 16 DEmRNAs at 24 h p.i.; 45 DElncRNAs, three DEmiRNAs and four DEmRNAs at 96 h p.i.; and 15 DElncRNAs, one DEmiRNAs and one DEmRNAs at 36 days p.i. (Fig. 6 and Supplementary Table S9).

4. Discussion

In the present study, we profiled the expression of lncRNAs, miRNAs, and mRNAs in the lung of Beagle dogs at 24 h, 96 h and 36 days p.i. by *T. canis*.

lncRNAs are regulatory RNA molecules, > 200 nucleotides, that do not code any proteins but can influence various biologic processes (Bin et al., 2018; Liu et al., 2018). lncRNAs are a mixture of classes with different biological mechanisms and/or functions

(Chen et al., 2016). They serve as ceRNAs by binding miRNAs and by interacting with specific miRNAs, lncRNAs can influence the regulation of adjacent target genes, in a cis- or trans-acting manner. In this study, a total of 1,570 annotated and 20,760 novel lncRNA transcripts were identified, including 1,012, 883 and 996 DElncRNA transcripts at 24 h p.i., 96 h p.i. and 36 days p.i., respectively. Large proportions of lncRNAs in dogs and other vertebrate species are not annotated because related mammalian taxa have different lncRNAs. Out of 1,898 lincRNAs expressed in human tissues, orthologous transcripts were found for 80% in chimpanzee, 63% in rhesus, 39% in cow, 38% in mouse, and 35% in rat, showing the significant differences between mammalian species (Washietl et al., 2014). Also, partially sequenced genomes, incomplete annotations of protein-coding genes, and shortcomings of tools used for assembly of full transcripts from short RNA-seq reads have all made direct lncRNA annotation challenging.

Because the functions of most lncRNAs identified in the present study are unknown, the predicted target genes of DElncRNAs were analyzed by GO and KEGG enrichment analyses to explore the functions of DElncRNAs. At 24 h p.i., 295 predicted target genes (e.g. *oasl*, *ubqln1* and *sox4*) of the DElncRNAs were significantly enriched in 66 immune- or inflammation-related GO terms (Supplementary Table S5), which are involved in the production and secretion of interleukins, interferons or other inflammatory responses. Oligoadenylate synthetase-like (OASL) can differentially regulate host interferon (IFN) responses during RNA and DNA virus infections, such as inhibiting RNA virus replication through enhancing IFN induction, while promoting DNA virus replication via inhibition of IFN induction (Zhu et al., 2014; Ghosh et al., 2019). OASL skewed the host immune response toward a niche that permits survival of *Mycobacterium leprae* (de Toledo-Pinto et al., 2016). These results suggest that OASL has paradoxical roles in host-pathogen interactions. The downregulation of *oasl* 2.6 times in our study, points to the possibility that an infection-related immunosuppressive effect makes the lung tissue more permissive to the survival and growth of *T. canis*.

Ubiquilin (UBQLN) proteins are important regulators of proteostasis, and downregulation of *ubqln1* was observed in primary human lung cancers (Beverly et al., 2012). *Ubqln1* was assigned to many immune response related GO terms in our study, and the level of *ubqln1* was downregulated 11 times at 24 h p.i., and the level of lncRNA XLOC_030813, located in the vicinity of the *ubqln1* gene, was significantly upregulated at 24 h p.i., suggesting that *ubqln1* may be regulated by lncRNA XLOC_030813 during *T. canis* infection. The transcriptional factor sex-determining region Y-box 4 (SOX4) preferentially regulates the

development of various organs, tissues, and lung cancers (Wang et al., 2015; Zhou et al., 2015). However, in the present study, the expression of *sox4* was decreased to 0 at 24 h p.i. However, the level of lncRNA XLOC_510697, located in the vicinity of the *sox4* gene, was upregulated 62.1 times. This result also suggests that upregulation of lncRNA XLOC_510697 causes inhibition of the expression of *sox4*, leading to a reduction in the healing of the injured lung tissues, paving the way for *T. canis* migration through the lung. The exact role of *oasl*, *ubqln1* and *sox4* in the pathogenesis of *T. canis* remains to be determined.

At 96 h p.i., 266 predicted target genes (e.g., *IL-21*, *bpifb1* and *runx1*) of DElncRNAs were significantly enriched in 77 immune- or inflammation-related GO terms (Supplementary Table S5). IL-21 promotes humoral immunity and increases IgG antibody production by B cells in the germinal center through restricting T follicular regulatory cell proliferation (Jandl et al., 2017). In the present study, the transcription of *IL-21* was significantly decreased to 0 at 96 h p.i., which could be one of the reasons why dogs cannot efficiently limit *T. canis* infection in the lung (Maizels, 2013). Interestingly, the expression level of lncRNA XLOC_237221, which is located in the vicinity of the *IL-21* gene, mirrored the expression of *IL-21* (i.e. decreased to 0 at 96 h p.i.). The concurrent downregulation of both lncRNA XLOC_237221 and *IL-21* deserves further investigation.

Bactericidal/permeability-increasing fold-containing B1 (BPIFB1) belongs to the BPIF family. The upregulation of genes in this family is accompanied by an abnormal inflammatory response in the lung (De Smet et al., 2018). The mRNA level of *bpifb1* is correlated with disease severity and was significantly upregulated in patients with stage III-IV chronic obstructive pulmonary disease (COPD) compared with stage II COPD patients or people without COPD (De Smet et al., 2018). Because BPIFB1 contains a domain that is similar to lipopolysaccharide (LPS)-binding protein, it participates in innate immune defense (Wei et al., 2018). The expression level of *bpifb1* was upregulated 26.6 times at 96 h p.i., suggesting that *T. canis* infection induces an inflammatory response in the lung or that the lung resists *T. canis* infection by upregulating the expression level of *bpifb1*. Therefore, *bpifb1* may have some relevance in the migration and development of *T. canis* in the lung, but this remains to be elucidated. Our analysis showed that the expression of lncRNA XLOC_347889, located in the vicinity of the *bpifb1* gene, was also increased by 13.4 times at 96 h p.i.

Runt-related transcription factor 1 (RUNX1) has a role in the inflammatory signaling pathway and plays a critical role in LPS-induced lung inflammation by regulating the NF-κB pathway (Tang et al., 2018). After LPS stimulation, *runx1*-deficient mice showed respiratory

exacerbation, inflammation and upregulation of pro-inflammatory cytokines, indicating that *runx1* deletion in alveolar epithelial cells promoted pulmonary inflammation (Tang et al., 2017). At 96 h p.i., most larvae of *T. canis* have reached or penetrated the lungs; however, no obvious clinical signs were observed in infected puppies. Therefore, it is likely that abnormal expression of *runx1* (upregulated 239.4 times) in lung plays important roles in inhibiting pro-inflammatory cytokines and lung injury repair after *T. canis* infection. Our analysis also showed that expression of lncRNA XLOC_462160, located in the vicinity of the *runx1* gene, was slightly increased at 96 h p.i.

At 36 days p.i., 327 predicted target genes (e.g. *bpifa1, gpnmb and slpi*) of DElncRNAs were significantly enriched in 75 immune- or inflammation-related GO terms (Supplementary Table S5). Similar to BPIFB1, BPIFA1 is an innate defense protein that participates in upper airway microbial infections (Bingle et al., 2011). For example, *bpifb1* and *bpifa1* were upregulated in COPD patients and correlated with disease severity (De Smet et al., 2018; Tsou et al., 2018). In the present study, *bpifa1* transcription level was remarkably upregulated 505.3 times at 24 h p.i., while its transcription level was downregulated 18.9 times at 36 days p.i. in the lung of infected dogs. Also, in contrast to BPIFB1, BPIFA1 participates in the regulation of airway surface liquid and ion transport (Hogg and Timens, 2009). Abnormal mucus rheology caused by, for example, enhanced epithelial sodium channel activity, resulted in an increased inflammatory response after bacterial infection, leading to a faster decline in lung function (Hogg and Timens, 2009). Therefore, the fact that *bpifa1* was upregulated at 24 h p.i., followed by a lack of significant expression at 96 h p.i., and was downregulated at 36 days p.i., is of particular relevance and suggests that upregulation of *bpifa1* at 24 h p.i. may pave the way for the subsequent migration of *T. canis* in the lung. lncRNA XLOC_347869, located in the vicinity of the *bpifa1* gene, was also significantly downregulated more than 13 times at 36 days p.i. Glycoprotein non-metastatic melanoma protein B (GPNMB) is a negative regulator of inflammatory responses in macrophages, and its deficiency resulted in severe colitis with elevated proinflammatory cytokines such as IL-6 (Sasaki et al., 2015). The low levels of *gpnmb* indirectly contributed to the expression of multiple inflammatory cytokines (e.g. IL-6) in Takayasu's arteritis (Kong et al., 2019). At 36 days p.i., the transcription *gpnmb* was increased 2.1 times, suggesting that upregulation of *gpnmb* may participate in the anti-inflammatory response at this stage of infection.

Secretory leukocyte protease inhibitor (SLPI) is an important regulator of innate and adaptive immune reaction. SLPI is induced by leukocyte products and inflammatory cytokines, however it can effectively inhibit the cascade reaction of inflammatory cytokines

(Majchrzak-Gorecka et al., 2016). For example, it interferes with the activity of NF-κB to counteract excessive inflammatory responses in lung diseases (Majchrzak-Gorecka et al., 2016). Low *slpi* expression in lung can affect lung function, causing severe asthma (Raundhal et al., 2015). In the present study, the transcription level of *slpi* was increased 7.1 times at 24 h p.i. and increased 3.8 times at 96 h p.i., which can protect lung tissue from over-inflammatory reaction caused by *T. canis* infection. However, the reason for its downregulation 2.7 times at 36 days p.i. needs further investigation. Therefore, the dynamic changes of *slpi* could play a role in balancing anti- and pro-inflammation responses to maintain lung function during *T. canis* infection. Our analysis also showed that the expression level of lncRNA XLOC_349131, which is located in the vicinity of the *slpi*, was decreased from a higher expression level to 0 at 36 days p.i.

We identified 49 common DEmRNAs between 24 h p.i. and 96 h p.i.; 55 common DEmRNAs between 96 h p.i. and 36 days p.i.; and 60 common DEmRNAs between 24 h p.i. and 36 days p.i. However, only 18 common DEmRNAs were identified at all infection stages (Fig. 3C), including *scgb1a1*, *dmbt1* and *slpi*. The secretoglobin family 1A member 1 (SCGB1A1) mediates cellular responses to inflammation and allergy (Kishore et al., 2006). The expansion of the *scgb1a1*+ cell population promotes lung regeneration during bacterial pneumonia (Khatri et al., 2019). As an important anti-inflammatory molecule, the transcription level of *scgb1a1* was remarkably upregulated > 100 times in all stages of infection, suggesting that persistent high expression of *scgb1a1* contributes to protection of the lung by attenuating the severity of the inflammatory response. The expression of *dmbt1* was upregulated in lung carcinomas, but was downregulated in tumor-flanking and inflammatory tissue (Mollenhauer et al., 2002). *Dmbt1* was upregulated 114.9 and 16.6 times at 24 h p.i. and 96 h p.i., respectively. However, it was downregulated 5.2 times at 36 days p.i. The dynamic change in the expression pattern of *slpi* was similar to that of *dmbt1*, suggesting that both genes may have a similar function.

At 24 h p.i., 39 DEmRNAs were significantly enriched in 10 signaling pathways such as legionellosis, pancreatic secretion and phagosome (Supplementary Table S7). One of the genes with a known function in the identified pathways was caspase-3 (Casp3), which is a cysteine protease that plays a role in apoptosis and inflammatory responses (Takashi et al., 2019). Upregulation of inflammatory genes, mild splenomegaly and renal inflammation were observed in *casp3*-deficient mice (Takashi et al., 2019). The downregulation of *casp3* was also linked to poor prognosis and chemoresistance in lung cancer (Okouoyo et al., 2004; Yoo et al., 2004). In this study, the expression of *casp3* was increased 15.6 times in lungs,

suggesting an anti-inflammatory role in *T. canis* infection.

At 96 h p.i., 19 DEmRNAs were significantly enriched in 12 signaling pathways such as pancreatic secretion, glutamatergic synapse and inflammatory mediator regulation of TRP channels (Supplementary Table S7). *IL-1β* is enriched in African trypanosomiasis and an inflammatory mediator regulation of TRP channels pathways. IL-1β has been suggested to play an important role in the inflammatory response during chronic obstructive pulmonary disease (COPD) pathogenesis (Yi et al., 2018). In our study, expression of *IL-1β* was decreased 5.6 times, suggesting that, as infection progresses, dogs limit the inflammatory reaction associated with *T. canis* infection.

At 36 days p.i., 41 DEmRNAs were significantly enriched in 10 signaling pathways including cytokine-cytokine receptor interaction, Jak-STAT signaling pathway and systemic lupus erythematosus (Supplementary Table S7). The upregulation of *IL-3RA*, *IL-21*, *IL-22RA2*, *IFN-γ*, *cish* (cytokine inducible SH2- containing protein) and *lif* (leukemia inhibitory factor) underpinned upregulation of the Jak-STAT signaling pathway at this stage of infection. IL-21 boosted humoral immunity and increased the expression of IgG (Jandl et al., 2017). Interestingly, the expression of *IL-21* was decreased to 0 at 96 h p.i.; however, it was upregulated 20.4 times at 36 days p.i., corresponding with detection of anti-*T. canis* IgG in infected puppies. The cytokine-cytokine receptor interaction pathway was also upregulated. Inflammatory cytokines (e.g. IFN-γ) can trigger the expression of inflammatory chemokines (e.g. CCL5) in tissue during inflammation and injury. In addition to the upregulation of *IL-21* by 20.4 times, *IFN-γ* was upregulated 8.9 times, *CCL5* was upregulated 5.2 times, and *CCR3*, the receptor of *CCL5*, was upregulated 7.6 times, demonstrating that although *T. canis* worms mainly resides in the intestinal tract at 36 days pi, they elicit inflammatory reactions in the lungs.

Metabolic pathways and the cytokine-cytokine receptor interaction pathway had the largest numbers of enriched DEmRNAs throughout the three infection stages (Table 2). *Toxocara canis* seems to impact lung immune responses in multiple ways, including modulation of cytokine production and chemokine signaling, and as a driver of inflammatory responses. This immune dysregulation was detected at all time points after infection, as described above. These results suggest that immune activation concurrent with metabolic alterations are important contributors to the pathogenesis of *T. canis* in the lung. The dual role of immunometabolism in the pathogenesis of *T. canis* infection of lung is in agreement with our previous global metabolomics profiling of sera from dogs infected by *T. canis* that identified alterations in serum steroid hormone biosynthesis pathway, which is known to have

an immunometabolic role (Zheng et al., 2019).

We also identified GO terms of the key DEmRNAs that were specifically related to immune response and/or inflammation. At 24 h p.i., 19 DEmRNAs were significantly enriched in 34 immunity- or inflammation-related GO terms, including 11 upregulated DEmRNAs and eight downregulated DEmRNAs (Supplementary Table S8). In addition to *slpi* and *scgb1a1*, the transcription level of forkhead box protein J1 (*foxj1*) was significantly upregulated > 4 times. FOXJ1 suppresses NF-κB transcription activity, and *foxj1*-deficient T cells increased NF-κB activity in vivo (Lin et al., 2004). FOXJ1 prevents autoimmunity and modulates inflammatory reactions by antagonizing pro-inflammatory transcriptional activities (Lin et al., 2004). FOXJ1 also limits activation of B cell and maturation of humoral responses (Lin et al., 2005). At 24 h p.i., upregulation of *foxj1* may facilitate the development and migration of *T. canis* larvae via attenuating the inflammatory and humoral immune responses.

At 96 h p.i., 44 DEmRNAs were significantly enriched in 124 immune response- or inflammation-related GO terms, including 20 upregulated DEmRNAs and 24 downregulated DEmRNAs (Supplementary Table S8). Thirty-six DEmRNAs were enriched in the GO term "immune system process". In addition to *bpifb1*, *scgb1a1*, *slpi* and *runx1*, the transcription level of pellino E3 ubiquitin protein ligase family member 3 (*peli3*) was significantly increased by 34.1 times. PELI3 was aberrantly upregulated in lung cancer, and high level of PELI3 was associated with poor prognosis; whereas deficiency of PELI3 significantly inhibited cell migration/invasion (He et al., 2019). The degradation of autophagy-dependent PELI3 inhibited the expression of pro-inflammatory IL-1β (Giegerich et al., 2014). In the present study, however, the upregulation of *peli3* and the downregulation of *IL-1β* occurred concurrently; therefore, the role of *peli3* in inflammatory or pro-inflammatory processes during *T. canis* infection of lungs still merits further investigation.

At 36 days p.i., 59 DEmRNAs were significantly enriched in 111 immune- or inflammatory-related GO terms, including 40 upregulated DEmRNAs and 19 downregulated DEmRNAs (Supplementary Table S8). Forty-four DEmRNAs participated in the GO term "immune system process" and 16 DEmRNAs participated in the GO term "inflammatory response". Endoplasmic reticulum aminopeptidase 2 (ERAP2) is an intracellular enzyme in the endoplasmic reticulum, which plays roles in influencing cellular cytotoxic immune responses and processing antigenic peptides (de Castro and Stratikos, 2019). Remarkably, the transcription level of *erap2* was increased 351.1 and 326.9 times with a roughly similar expression pattern at 96 h p.i. and 36 days p.i., respectively, suggesting that immunoinflammatory responses continue to occur in the lung from 96 h p.i. to 36 days p.i.

ADAMTS 12 is necessary for inflammation, and *adamts 12*-deficient mice showed a reduction in neutrophil apoptosis and an increase in inflammatory response (Moncada-Pazos et al., 2012). Therefore, upregulation of *adamts 12* by 402.6 times suggests an anti-inflammatory process at 36 days p.i. CC motif chemokine ligand 5 (CCL5) that inhibits LPS-induced activation of NF-κB and JNK pathways (Bai et al., 2018), was upregulated 5.2 times in the present study. Overexpression of *CCL5* was identified in LPS-treated human fetal lung fibroblast WI-38 cells, however silencing *CCL5* can protect WI-38 cells from LPS-induced inflammatory damage by inhibiting cell apoptosis, increasing cell viability and reducing the production of pro-inflammatory cytokines (Bai et al., 2018). The identification of many immune- or inflammation-related mRNAs at 36 days p.i. suggest that the inflammatory responses elicited by *T. canis* continue even after the worms reside in the intestine. On the other hand, lungs produce molecules to support an anti-inflammatory response and self-repair at 36 days p.i. Maintaining such a balance between cell-mediated and humoral immune responses is essential to limit lung damage.

At 24 h p.i., ceRNA network analysis showed that 45 DElncRNAs and 16 DEmRNAs were targeted by three miRNAs (Fig. 6A and Supplementary Table S9). The expression of miRNA-423a increased significantly in dogs with lymphoma (Fujiwara-Igarashi et al., 2015). In this study, the expression of homeodomain-containing gene 10 (*hoxc10*) was decreased to 0 in infected lungs. The level of prostate stem cell antigen (*psca*) was upregulated 16 times, which seems to be correlated with downregulation of miR-novel_405 and a variety of downregulated lncRNA (Fig. 6A). PSCA has immune-modulatory properties in a tumor microenvironment (Liu et al., 2017) and its downregulation promoted *Helicobacter pylori*-induced severe gastritis (Toyoshima et al., 2018). Thus, upregulation of *psca* may represent an anti-parasitic mechanism. The transcription of *foxj1* was upregulated > 4 times at 24 h p.i.. FOXJ1 prevents autoimmunity and modulates inflammatory reactions by suppressing NF-κB transcription activity (Lin et al., 2004). FOXJ1 also limits the activation of B cell and maturation of humoral responses (Lin et al., 2005). The upregulation of *foxj1* may be influenced by the downregulation of miRNA-423a and miR-novel_405, which may have been affected by many down-regulated lncRNAs. The specific function of *hoxc10, psca and foxj1* in relation to the associated miRNAs and lncRNAs in the context of *T. canis* infection merits further investigation.

At 96 h p.i., 45 DElncRNAs and four DEmRNAs were targeted by three DEmiRNAs (Fig. 6B and Supplementary Table S9). Crk-associated substrate scaffolding protein family member 4 (CASS4) is a member of the CAS family that participates in the regulation of cell

attachment, migration and invasion (Tikhmyanova et al., 2010; Nikonova et al., 2014). In this study, *Cass4* and miRNA-28 were upregulated 27.9 and 1.94 times at 96 h p.i., respectively. The expression and biological functions of miRNA-28 have been investigated in many cancers and it was found to promote cell proliferation and invasion in gastric cancer (Li et al., 2016; Li et al., 2018). However, the roles of *cass4* and miRNA-28 in *T. canis* infection remain to be determined. Solute carrier family 12 member 7 (SLC12A7) and solute carrier family 26 member 3 (SLC26A3) are the members of solute carrier family that influence various physiological and pathophysiological functions (Sai and Tsuji, 2004). SLC26A3 mediates intestinal NaCl absorption and is downregulated in inflammatory bowel disease-associated diarrhea (Chatterjee et al., 2017). Impaired chloride absorption caused by downregulation of *slc26a3* contributed to *Cryptosporidium parvum*-induced acute and self-limiting diarrhea (Kumar et al., 2019). The expression of *slc26a3* at 96 h p.i. decreased to 0. What role the decrease in *slc26a3* played in the crosstalk between the lung and *T. canis* remains to be investigated. Interestingly, the transcription level of *slc12a7* was upregulated 3.5 times. *Slc26a3* was targeted by miRNA-493, while *slc12a7* was targeted by miRNA-novel_500, which may have underpinned the differential expression of *slc12a7* and *slc26a3*. Our results showed that the level of miRNA-493 was upregulated two times at 96 h p.i. Previous results suggest that higher expression of miRNA-493 is beneficial to the host. For example, downregulation of miRNA-493 promoted melanoma proliferation (Cui et al., 2017) and epigenetic silencing of miRNA-493 increased lung cancer resistance to cisplatin (Gu et al., 2017). Also, breast cancer patients had better survival with high expression of miRNA-493 (Yao et al., 2018).

At 36 days p.i., only 15 DElncRNAs and one DEmRNA were targeted by one DEmiRNA (Fig. 6C and Supplementary Table S9). The miRNA-150 was upregulated 1.5 times. miRNA-150 is a regulator of the differentiation and activation of immune cells, such as B cells, T cells and NK cells (Bezman et al., 2011; He et al., 2013), and is involved in the PI3K-AKT pathway (Mei and Zhang, 2019). Overexpression of miR-150 significantly inhibited proliferation, migration, and invasion of melanoma cells (Sun et al., 2019). The role of miRNA-150 in *T. canis* infection remains to be elucidated.

In summary, to our knowledge for the first time, we report the results of a comprehensive analysis of the expression profiles of lncRNAs, miRNAs, and mRNAs in the lung of Beagle dogs experimentally infected by *T. canis*. The transcriptional changes were dominated by differentially expressed transcripts involved in the immune and/or inflammatory response. The transcription of the anti-inflammatory *scgb1a1* was increased >

100 times at all infection stages, suggesting that *scgb1a1* plays a key role in regulating lung tolerance to *T. canis* through the entire infection period. Also, the upregulation of *foxj1* at 24 h p.i. and downregulation of *IL-1β* and *IL-21* at 96 h p.i. play roles in the attenuation of humoral immunity. These data suggest that both cell-mediated and humoral immune responses contribute to the mediation of *T. canis* infection of the lung. ceRNA network analysis revealed significant correlations among DElncRNAs, DEmiRNAs and DEmRNAs, and identified new endogenous miRNA sponges that are involved in the pathogenesis of *T. canis*. It is hoped that these large-scale expression profiling data will promote further investigations by providing numerous *T. canis*-dysregulated lncRNAs, mRNAs and miRNAs, and pathways that represent promising candidates for disease biomarkers and/or therapeutic targets.

Acknowledgments

Project support was provided by the Elite Program of Chinese Academy of Agricultural Sciences and the Agricultural Science and Technology Innovation Program (ASTIP) (grant no. CAAS-ASTIP-2016-LVRI-03). We thank Novogene Bioinformatics Technology Co., Ltd (Beijing, China) for performing the sequencing and preliminary data analysis.

Appendix A. Supplementary Data

Supplementary data to this article can be found online at:

References

Anders, S., Pyl, P.T., Huber, W., 2015. HTSeq--a Python framework to work with high-throughput sequencing data. Bioinformatics 31, 166–169.

Bai, D., Han, A., Cong, S., 2018. The effect of down-regulation of CCL5 on lipopolysaccharide-induced WI-38 fibroblast injury: a potential role for infantile pneumonia. Iran. J. Basic. Med. Sci. 21, 449–454.

Beverly, L.J., Lockwood, W.W., Shah, P.P., Erdjument-Bromage, H., Varmus, H., 2012. Ubiquitination, localization, and stability of an anti-apoptotic BCL2-like protein, BCL2L10/BCLb, are regulated by Ubiquilin1. Proc. Natl. Acad. Sci. U. S. A. 109, E119–126.

Bezman, N.A., Tirtha, C., Timothy, B., Lanier, L.L., 2011. miR-150 regulates the development of NK and iNKT cells. J. Exp. Med. 208, 2717–2731.

Bin, X., Hongjian, Y., Xiping, Z., Bo, C., Shifeng, Y., Binbin, T., 2018. Research progresses in roles of LncRNA and its relationships with breast cancer. Cancer Cell Int. 18, 179.

Bingle, C.D., Seal, R.L., Craven, C.J., 2011. Systematic nomenclature for the PLUNC/PSP/BSP30/SMGB proteins as a subfamily of the BPI fold-containing superfamily. Biochem. Soc. Trans. 39, 977–983.

Chatterjee, I., Kumar, A., Castilla-Madrigal, R.M.a., Pellon-Cardenas, O., Gill, R.K., Alrefai, W.A., Borthakur, A., Verzi, M., Dudeja, P.K., 2017. CDX2 upregulates SLC26A3 gene expression in intestinal epithelial cells. Am. J. Physiol. Gastrointest. Liver Physiol. 313.

Chen, J., Liu, Q., Liu, G.H., Zheng, W.B., Hong, S.J., Sugiyama, H., Zhu, X.Q., Elsheikha, H.M., 2018. Toxocariasis: a silent threat with a progressive public health impact. Infect Dis Poverty 7, 13.

Chen, J., Shishkin, A.A., Zhu, X., Kadri, S., Maza, I., Guttman, M., Hanna, J.H., Regev, A., Garber, M., 2016. Evolutionary analysis across mammals reveals distinct classes of long non-coding RNAs. Genome Biol. 17, 19.

Craig, J.M., Scott, A.L., 2014. Helminths in the lungs. Parasite Immunol. 36, 463–474.

Cui, A., Jin, Z., Gao, Z., Jin, M., Zhu, L., Li, L., Jin, C., An, Y., 2017. Downregulation of

722 miR-493 promoted melanoma proliferation by suppressing IRS4 expression. Tumour Biol.
723 39, 1010428317701640.
724 de Castro, J.A.L., Stratikos, E., 2019. Intracellular antigen processing by ERAP2: Molecular
725 mechanism and roles in health and disease. Hum. Immunol. 80, 310–317.
726 De Smet, E.G., Seys, L.J., Verhamme, F.M., Vanaudenaerde, B.M., Brusselle, G.G., Bingle,
727 C.D., Bracke, K.R., 2018. Association of innate defense proteins BPIFA1 and BPIFB1
728 with disease severity in COPD. Int. J. Chron. Obstruct. Pulmon. Dis. 13, 11–27.
729 de Toledo-Pinto, T.G., Ferreira, A.B., Ribeiro-Alves, M., Rodrigues, L.S., Batista-Silva, L.R.,
730 Silva, B.J., Lemes, R.M., Martinez, A.N., Sandoval, F.G., Alvarado-Arnez, L.E., Rosa,
731 P.S., Shannon, E.J., Pessolani, M.C., Pinheiro, R.O., Antunes, S.L., Sarno, E.N., Lara, F.A.,
732 Williams, D.L., Ozorio Moraes, M., 2016. STING-dependent 2'-5' oligoadenylate
733 synthetase-like production is required for intracellular mycobacterium leprae survival. J.
734 Infect. Dis. 214, 311–320.
735 Enright, A.J., John, B., Gaul, U., Tuschl, T., Sander, C., Marks, D.S., 2003. MicroRNA targets
736 in drosophila. Genome Biol. 5, R1.
737 Fakhri, Y., Gasser, R.B., Rostami, A., Fan, C.K., Ghasemi, S.M., Javanian, M., Bayani, M.,
738 Armoon, B., Moradi, B., 2018. *Toxocara* eggs in public places worldwide - A systematic
739 review and meta-analysis. Environ Pollut. 242, 1467–1475.
740 Friedlander, M.R., Mackowiak, S.D., Li, N., Chen, W., Rajewsky, N., 2012. miRDeep2
741 accurately identifies known and hundreds of novel microRNA genes in seven animal
742 clades. Nucleic Acids Res. 40, 37–52.
743 Fujiwara-Igarashi, A., Igarashi, H., Mizutani, N., Goto-Koshino, Y., Takahashi, M., Ohno, K.,
744 Tsujimoto, H., 2015. Expression profile of circulating serum microRNAs in dogs with
745 lymphoma. Vet. J. 205, 317–321.
746 Ghosh, A., Shao, L., Sampath, P., Zhao, B., Patel, N.V., Zhu, J., Behl, B., Parise, R.A.,
747 Beumer, J.H., O'Sullivan, R.J., DeLuca, N.A., Thorne, S.H., Rathinam, V.A.K., Li, P.,
748 Sarkar, S.N., 2019. Oligoadenylate-synthetase-family protein OASL inhibits activity of
749 the DNA sensor cGAS during DNA virus infection to limit interferon production.
750 Immunity 50, 51–63.e55.
751 Giegerich, A.K., Kuchler, L., Sha, L.K., Knape, T., Heide, H., Wittig, I., Behrends, C., Brune,

B., von Knethen, A., 2014. Autophagy-dependent PELI3 degradation inhibits proinflammatory IL1B expression. Autophagy 10, 1937–1952.

Gu, Y., Zhang, Z., Yin, J., Ye, J., Song, Y., Liu, H., Xiong, Y., Lu, M., Zheng, G., He, Z., 2017. Epigenetic silencing of miR-493 increases the resistance to cisplatin in lung cancer by targeting tongue cancer resistance-related protein 1(TCRP1). J Exp Clin Cancer Res 36, 114.

He, L., Zhang, A., Chu, P., Li, Y., Huang, R., Liao, L., Zhu, Z., Wang, Y., 2017. Deep illumina sequencing reveals conserved and novel microRNAs in grass carp in response to grass carp reovirus infection. BMC Genomics 18, 195.

He, Y., Jiang, X., Chen, J., 2013. The role of miR-150 in normal and malignant hematopoiesis. Oncogene 33, 3887–3893.

He, Y., Shi, Y., Liu, R., Wang, Z., Wang, B., Li, S., Zhang, H., 2019. PELI3 mediates pro-tumor actions of down-regulated miR-365a-5p in non-small cell lung cancer. Biol. Res. 52, 24.

Hogg, J.C., Timens, W., 2009. The pathology of chronic obstructive pulmonary disease. Annu. Rev. Pathol. 4, 435–459.

Jandl, C., Liu, S.M., Canete, P.F., Warren, J., Hughes, W.E., Vogelzang, A., Webster, K., Craig, M.E., Uzel, G., Dent, A., Stepensky, P., Keller, B., Warnatz, K., Sprent, J., King, C., 2017. IL-21 restricts T follicular regulatory T cell proliferation through Bcl-6 mediated inhibition of responsiveness to IL-2. Nat. Commun. 8, 14647.

Janecek, E., Wilk, E., Schughart, K., Geffers, R., Strube, C., 2015. Microarray gene expression analysis reveals major differences between *Toxocara canis* and *Toxocara cati* neurotoxocarosis and involvement of *T. canis* in lipid biosynthetic processes. Int. J. Parasitol. 45, 495–503.

Kang, Y.J., Yang, D.C., Kong, L., Hou, M., Meng, Y.Q., Wei, L., Gao, G., 2017. CPC2: a fast and accurate coding potential calculator based on sequence intrinsic features. Nucleic Acids Res. 45, W12–W16.

Khatri, A., Kraft, B.D., Tata, P.R., Randell, S.H., Piantadosi, C.A., Pendergast, A.M., 2019. ABL kinase inhibition promotes lung regeneration through expansion of an SCGB1A1+ SPC+ cell population following bacterial pneumonia. Proc. Natl. Acad. Sci. U. S. A. 116,

1603–1612.

Kishore, U., Greenhough, T.J., Waters, P., Shrive, A.K., Ghai, R., Kamran, M.F., Bernal, A.L., Reid, K.B., Madan, T., Chakraborty, T., 2006. Surfactant proteins SP-A and SP-D: structure, function and receptors. Mol. Immunol. 43, 1293–1315.

Kong X., Sawalha A.H., 2019. Takayasu arteritis risk locus in IL6 represses the anti-inflammatory gene GPNMB through chromatin looping and recruiting MEF2–HDAC complex. Ann. Rheum. Dis. 78, 1388–1397.

Kumar, A., Jayawardena, D., Anbazhagan, A.N., Chatterjee, I., Priyamvada, S., Alrefai, W.A., Borthakur, A., Dudeja, P.K., 2019. Decreased SLC26A3 expression and function in intestinal epithelial cells in response to *cryptosporidiium parvum* infection. Am. J. Physiol. Cell Physiol. 317, C1205–C1212.

Kuzucu, A., 2006. Parasitic diseases of the respiratory tract. Curr. Opin. Pulm. Med. 12, 212–221.

Langmead, B., Salzberg, S.L., 2012. Fast gapped-read alignment with Bowtie 2. Nat. Methods 9, 357–359.

Langmead, B., Trapnell, C., Pop, M., Salzberg, S.L., 2009. Ultrafast and memory-efficient alignment of short DNA sequences to the human genome. Genome Biol. 10, R25.

Li, A., Zhang, W., Xia, H., Miao, Y., Zhou, H., Zhang, X., Dong, Q., Li, Q., Qiu, X., Wang, E., 2016. Overexpression of CASS4 promotes invasion in non-small cell lung cancer by activating the AKT signaling pathway and inhibiting E-cadherin expression. Tumour Biol. 37, 15157–15164.

Li, L., Zhu, X., Shou, T., Yang, L., Cheng, X., Wang, J., Deng, L., Zheng, Y., 2018. MicroRNA-28 promotes cell proliferation and invasion in gastric cancer via the PTEN/PI3K/AKT signalling pathway. Mol. Med. Rep. 17, 4003–4010.

Lin, L., Brody, S.L., Peng, S.L., 2005. Restraint of B cell activation by Foxj1-mediated antagonism of NF-kappa B and IL-6. J. Immunol. 175, 951–958.

Lin, L., Spoor, M.S., Gerth, A.J., Brody, S.L., Peng, S.L., 2004. Modulation of Th1 activation and inflammation by the NF-kappaB repressor Foxj1. Science 303, 1017–1020.

Liu, L., Li, E., Luo, L., Zhao, S., Li, F., Wang, J., Luo, J., Zhao, Z., 2017. PSCA regulates IL-6 expression through p38/NF-kappaB signaling in prostate cancer. Prostate 77,

1389–1400.

Liu, T.L., Fan, X.C., Li, Y.H., Yuan, Y.J., Yin, Y.L., Wang, X.T., Zhang, L.X., Zhao, G.H., 2018. Expression profiles of mRNA and lncRNA in HCT-8 cells infected with *cryptosporidium parvum* IId subtype. Front. Microbiol. 9, 1409.

Lotia, S., Montojo, J., Dong, Y., Bader, G.D., Pico, A.R., 2013. Cytoscape app store. Bioinformatics 29, 1350–1351.

Love, M.I., Huber, W., Anders, S., 2014. Moderated estimation of fold change and dispersion for RNA-seq data with DESeq2. Genome Biol. 15, 550.

Ma, G., Holland, C.V., Wang, T., Hofmann, A., Fan, C.K., Maizels, R.M., Hotez, P.J., Gasser, R.B., 2018. Human toxocariasis. Lancet Infect. Dis. 18, e14–e24.

Maizels, R.M., 2013. *Toxocara canis*: molecular basis of immune recognition and evasion. Vet. Parasitol. 193, 365–374.

Majchrzak-Gorecka, M., Majewski, P., Grygier, B., Murzyn, K., Cichy, J., 2016. Secretory leukocyte protease inhibitor (SLPI), a multifunctional protein in the host defense response. Cytokine Growth Factor Rev. 28, 79–93.

Mei, M., Zhang, M., 2019. Non-coding RNAs in natural killer/T-cell lymphoma. Front. Oncol. 9, 515.

Mikaeili, F., Mathis, A., Deplazes, P., Mirhendi, H., Barazesh, A., Ebrahimi, S., Kia, E.B., 2017. Differentiation of *Toxocara canis* and *Toxocara cati* based on PCR-RFLP analyses of rDNA-ITS and mitochondrial cox1 and nad1 regions. Acta Parasitol. 62, 549–556.

Mollenhauer, J., Helmke, B., Muller, H., Kollender, G., Lyer, S., Diedrichs, L., Holmskov, U., Ligtenberg, T., Herbertz, S., Krebs, I., Wiemann, S., Madsen, J., Bikker, F., Schmitt, L., Otto, H.F., Poustka, A., 2002. Sequential changes of the DMBT1 expression and location in normal lung tissue and lung carcinomas. Genes Chromosomes Cancer 35, 164–169.

Moncada-Pazos, A., Obaya, A.J., Llamazares, M., Heljasvaara, R., Suarez, M.F., Colado, E., Noel, A., Cal, S., Lopez-Otin, C., 2012. ADAMTS-12 metalloprotease is necessary for normal inflammatory response. J. Biol. Chem. 287, 39554–39563.

Moxon, S., Schwach, F., Dalmay, T., Maclean, D., Studholme, D.J., Moulton, V., 2008. A toolkit for analysing large-scale plant small RNA datasets. Bioinformatics 24, 2252–2253.

Nikonova, A.S., Gaponova, A.V., Kudinov, A.E., Golemis, E.A., 2014. CAS proteins in health

and disease: an update. IUBMB Life 66, 387–395.

Okouoyo, S., Herzer, K., Ucur, E., Mattern, J., Krammer, P.H., Debatin, K.M., Herr, I., 2004. Rescue of death receptor and mitochondrial apoptosis signaling in resistant human NSCLC in vivo. Int. J. Cancer 108, 580–587.

Pertea, M., Kim, D., Pertea, G.M., Leek, J.T., Salzberg, S.L., 2016. Transcript-level expression analysis of RNA-seq experiments with HISAT, StringTie and Ballgown. Nat. Protoc. 11, 1650–1667.

Punta, M., Coggill, P.C., Eberhardt, R.Y., Mistry, J., Tate, J., Boursnell, C., Pang, N., Forslund, K., Ceric, G., Clements, J., Heger, A., Holm, L., Sonnhammer, E.L., Eddy, S.R., Bateman, A., Finn, R.D., 2012. The Pfam protein families database. Nucleic Acids Res. 40, D290–301.

Raundhal, M., Morse, C., Khare, A., Oriss, T.B., Milosevic, J., Trudeau, J., Huff, R., Pilewski, J., Holguin, F., Kolls, J., Wenzel, S., Ray, P., Ray, A., 2015. High IFN-gamma and low SLPI mark severe asthma in mice and humans. J. Clin. Invest. 125, 3037–3050.

Regis, S.C., Mendonça, L.R., Silva Ndos, S., Dattoli, V.C., Alcântara-Neves, N.M., Barrouin-Melo, S.M., 2011. Seroprevalence and risk factors for canine toxocariasis by detection of specific IgG as a marker of infection in dogs from Salvador, Brazil. Acta Trop. 120, 46–51.

Sai, Y., Tsuji, A., 2004. Transporter-mediated drug delivery: recent progress and experimental approaches. Drug Discov. Today 9, 712–720.

Sasaki, F., Kumagai, K., Uto, H., Takami, Y., Kure, T., Tabu, K., Nasu, Y., Hashimoto, S., Kanmura, S., Numata, M., Moriuchi, A., Sakiyama, T., Tsubouchi, H., Ido, A., 2015. Expression of glycoprotein nonmetastatic melanoma protein B in macrophages infiltrating injured mucosa is associated with the severity of experimental colitis in mice. Mol. Med. Rep. 12, 7503–7511.

Sun, L., Luo, H., Bu, D., Zhao, G., Yu, K., Zhang, C., Liu, Y., Chen, R., Zhao, Y., 2013. Utilizing sequence intrinsic composition to classify protein-coding and long non-coding transcripts. Nucleic Acids Res. 41, e166.

Sun, X., Zhang, C., Cao, Y., Liu, E., 2019. miR-150 suppresses tumor growth in melanoma through downregulation of MYB. Oncol. Res. 27, 317–323.

Takamiya, S., Mita, T., 2016. Large-scale purification of active liquid-cultured *Caenorhabditis elegans* using a modified Baermann apparatus. Parasitol. Int. 65, 580–583.

Takashi, S., Osamu, I., Teppei, N., Taro, H., Ali, E.Y.H., Yasuhiro, K., 2019. Immune-associated renal disease found in caspase 3-deficient mice. Cell Tissue Res. 379, 323–335.

Tang, X., Sun, L., Jin, X., Chen, Y., Zhu, H., Liang, Y., Wu, Q., Han, X., Liang, J., Liu, X., Liang, Z., Wang, G., Luo, F., 2017. Runt-related transcription factor 1 regulates LPS-induced acute lung injury via NF-kappaB signaling. Am. J. Respir. Cell Mol. Biol. 57, 174–183.

Tang, X., Sun, L., Wang, G., Chen, B., Luo, F., 2018. RUNX1: a regulator of NF-kB signaling in pulmonary diseases. Curr. Protein Pept. Sci. 19, 172–178.

Tikhmyanova, N., Little, J.L., Golemis, E.A., 2010. CAS proteins in normal and pathological cell growth control. Cell. Mol. Life Sci. 67, 1025–1048.

Toyoshima, O., Tanikawa, C., Yamamoto, R., Watanabe, H., Yamashita, H., Sakitani, K., Yoshida, S., Kubo, M., Matsuo, K., Ito, H., Koike, K., Seto, Y., Matsuda, K., 2018. Decrease in PSCA expression caused by *Helicobacter pylori* infection may promote progression to severe gastritis. Oncotarget 9, 3936–3945.

Tsou, Y.A., Tung, M.C., Alexander, K.A., Chang, W.D., Tsai, M.H., Chen, H.L., Chen, C.M., 2018. The role of BPIFA1 in upper airway microbial infections and correlated diseases. Biomed Res. Int. 2018, 2021890.

Wang, D., Hao, T., Pan, Y., Qian, X., Zhou, D., 2015. Increased expression of SOX4 is a biomarker for malignant status and poor prognosis in patients with non-small cell lung cancer. Mol. Cell. Biochem. 402, 75–82.

Washietl, S., Kellis, M., Garber, M., 2014. Evolutionary dynamics and tissue specificity of human long noncoding RNAs in six mammals. Genome Res. 24, 616–628.

Webster, G.A., 1958. A report on *Toxocara canis* Werner, 1782. Can. J. Comp. Med. Vet. Sci. 22, 272–279.

Wei, F., Tang, L., He, Y., Wu, Y., Shi, L., Xiong, F., Gong, Z., Guo, C., Li, X., Liao, Q., Zhang, W., Ni, Q., Luo, J., Li, X., Li, Y., Peng, C., Chen, X., Li, G., Xiong, W., Zeng, Z., 2018. BPIFB1 (LPLUNC1) inhibits radioresistance in nasopharyngeal carcinoma by inhibiting

VTN expression. Cell Death Dis. 9, 432.

Wen, M., Shen, Y., Shi, S., Tang, T., 2012. miREvo: an integrative microRNA evolutionary analysis platform for next-generation sequencing experiments. BMC Bioinformatics 13, 140.

Wu, J., Mao, X., Cai, T., Luo, J., Wei, L., 2006. KOBAS server: a web-based platform for automated annotation and pathway identification. Nucleic Acids Res. 34, W720–724.

Yao, L., Liu, Y., Cao, Z., Li, J., Huang, Y., Hu, X., Shao, Z., 2018. MicroRNA-493 is a prognostic factor in triple-negative breast cancer. Cancer Sci. 109, 2294–2301.

Yi, G., Liang, M., Li, M., Fang, X., Liu, J., Lai, Y., Chen, J., Yao, W., Feng, X., Hu, Lin, C., Zhou, X., Liu, Z., 2018. A large lung gene expression study identifying IL1B as a novel player in airway inflammation in COPD airway epithelial cells. Inflamm. Res. 67, 539–551.

Yoo, J., Kim, C.H., Song, S.H., Shim, B.Y., Jeong, Y.J., Ahn, M.I., Kim, S., Cho, D.G., Jo, M.S., Cho, K.D., Cho, H.J., Kang, S.J., Kim, H.K., 2004. Expression of caspase-3 and c-myc in non-small cell lung cancer. Cancer Res. Treat. 36, 303–307.

Young, M.D., Wakefield, M.J., Smyth, G.K., Oshlack, A., 2010. Gene ontology analysis for RNA-seq: accounting for selection bias. Genome Biol. 11, R14.

Zhang, T., Xi, Q., Wang, D., Li, J., Wang, M., Li, D., Zhu, L., Jin, L., 2019. Mitochondrial dysfunction and endoplasmic reticulum stress involved in oocyte aging: an analysis using single-cell RNA-sequencing of mouse oocytes. J. Ovarian Res. 12, 53.

Zheng, W.B., Zou, Y., Elsheikha, H.M., Liu, G.H., Hu, M.H., Wang, S.L., Zhu, X.Q., 2019. Serum metabolomic alterations in Beagle dogs experimentally infected with *Toxocara canis*. Parasit. Vectors 12, 447.

Zheng, W.B., Zou, Y., Zhu, X.Q., Liu, G.H., 2020. *Toxocara* “omics” and the promises it holds for medicine and veterinary medicine. Adv. Parasitol. 109, 89–108.

Zhou, J., Xiong, Q., Chen, H., Yang, C., Fan, Y., 2017. Identification of the spinal expression profile of non-coding RNAs involved in neuropathic pain following spared nerve injury by sequence analysis. Front. Mol. Neurosci. 10, 91.

Zhou, L., Chen, J., Li, Z., Li, X., Hu, X., Huang, Y., Zhao, X., Liang, C., Wang, Y., Sun, L., Shi, M., Xu, X., Shen, F., Chen, M., Han, Z., Peng, Z., Zhai, Q., Chen, J., Zhang, Z., Yang,

R., Ye, J., Guan, Z., Yang, H., Gui, Y., Wang, J., Cai, Z., Zhang, X., 2010. Integrated profiling of microRNAs and mRNAs: microRNAs located on Xq27.3 associate with clear cell renal cell carcinoma. PLoS One 5, e15224.

Zhou, Y., Wang, X., Huang, Y., Chen, Y., Zhao, G., Yao, Q., Jin, C., Huang, Y., Liu, X., Li, G., 2015. Down-regulated SOX4 expression suppresses cell proliferation, metastasis and induces apoptosis in Xuanwei female lung cancer patients. J. Cell. Biochem. 116, 1007–1018.

Zhu, J., Zhang, Y., Ghosh, A., Cuevas, R.A., Forero, A., Dhar, J., Ibsen, M.S., Schmid-Burgk, J.L., Schmidt, T., Ganapathiraju, M.K., Fujita, T., Hartmann, R., Barik, S., Hornung, V., Coyne, C.B., Sarkar, S.N., 2014. Antiviral activity of human OASL protein is mediated by enhancing signaling of the RIG-I RNA sensor. Immunity 40, 936–948.

Zhu, X.Q., Korhonen, P.K., Cai, H., Young, N.D., Nejsum, P., von Samson-Himmelstjerna, G., Boag, P.R., Tan, P., Li, Q., Min, J., Yang, Y., Wang, X., Fang, X., Hall, R.S., Hofmann, A., Sternberg, P.W., Jex, A.R., Gasser, R.B., 2015. Genetic blueprint of the zoonotic pathogen *Toxocara canis*. Nat. Commun. 6, 6145.

Legends to figures

Fig. 1. The number of eosinophils in the blood of *Toxocara canis*-infected and control Beagle dogs at the three indicated time points p.i. The graph represents the means and standard deviations of the results determined for three dogs per group.

Fig. 2. The workflow of data processing. First, long non-coding RNAs (lncRNAs), mRNA and microRNAs (miRNAs) were obtained by sequencing and the differentially expressed (DE) transcripts of lncRNA, mRNA and miRNA were determined in the lung of Beagle dogs at different stages of *Toxocara canis* infection. Then, Gene Ontology (GO) terms and Kyoto Encyclopedia of Genes and Genomes (KEGG) pathways of the targeted genes of differentially expressed (DE) lncRNAs, and DEmRNAs were analyzed. The immune- or inflammation-related GO terms based on the target genes of differentially expressed (DE) lncRNAs and DEmRNAs were also analyzed to identify the function of the most significantly enriched genes. Increased and decreased expression of the transcripts are indicated by red upward pointing arrows and blue downward pointing arrows, respectively.

Fig. 3. Comparisons of long non-coding RNAs (lncRNAs), mRNAs and microRNAs (miRNAs) differentially expressed in the lung of Beagle dogs 24 h, 96 h and 36 days after *Toxocara canis* infection. (A) The numbers of differentially expressed (DE) lncRNAs, DEmRNAs and DEmiRNAs in three infection stages. Sky blue represents the total number of DE transcripts. Red and blue colors represent upregulated and downregulated transcripts, respectively. (B-D) Venn diagrams showing the common and unique DElncRNAs, DEmRNAs and DEmiRNAs at three infection time points between infected and control groups, respectively.

Fig. 4. Verification of the expression of (A-E) five differentially expressed (DE) mRNAs, (F-H) three DE long non-coding RNAs (lncRNAs) and (I) 10 DE microRNAs (miRNAs) by quantitative real-time PCR (qRT-PCR) in the lung of Beagle dogs at different stages of *Toxocara canis* infection. The Y-axis denotes the $\log_2$ fold change and the X-axis represents different time points p.i. The error bars represent the S.D. based on three replicates. The qRT-PCR verification of the 18 transcripts demonstrated an overall similarity in the

magnitude and direction of the expression measured by RNA sequencing and qRT-PCR.

Fig. 5. Scatter plots of the top 20 enriched Kyoto Encyclopedia of Genes and Genomes (KEGG) pathways of the differentially expressed (DE) mRNAs at (A) 24 h p.i., (B) 96 h p.i. and (C) 36 days p.i. in the lung of Beagle dogs at different stages of *Toxocara canis* infection. The Y-axis label shows the KEGG pathway name. Dot size represents the number of DEmRNAs in the pathway (bigger dots indicate large DEmRNA numbers). The colours of the dots represent the *P* values of enrichment, with red indicating high enrichment, while green indicates low enrichment.

Fig. 6. The competing endogenous RNA (ceRNA) networks at (A) 24 h p.i., (B) 96 h p.i. and (C) 36 days p.i. in the lung of Beagle dogs at different stages of *Toxocara canis* infection. The differentially expressed (DE) mRNAs, DE long non-coding RNAs (lncRNAs) and DE microRNAs (miRNAs) are denoted by diamonds, ellipses, rectangles, respectively. Red and green colors represent upregulated and downregulated transcripts, respectively. Grey edges indicate DElncRNA-DEmiRNA-DEmRNA interactions. In each ceRNA network, a single centrally located miRNA mediates the interactions between the RNAs.

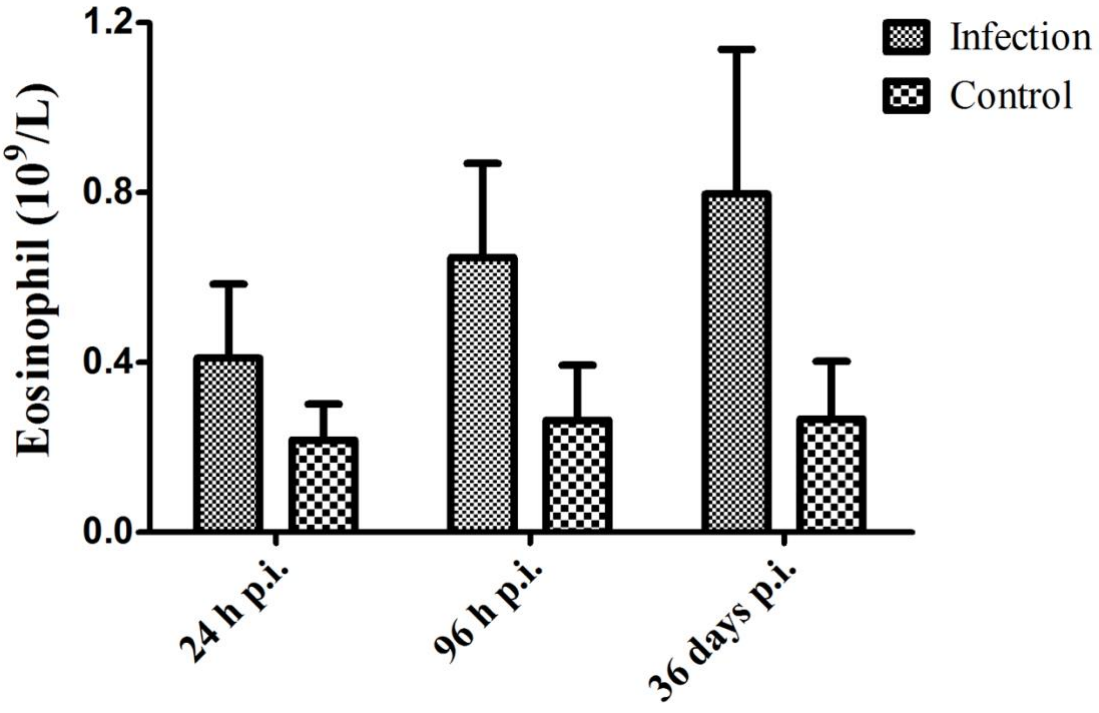

1001

1002 **Figure 1.**

1003

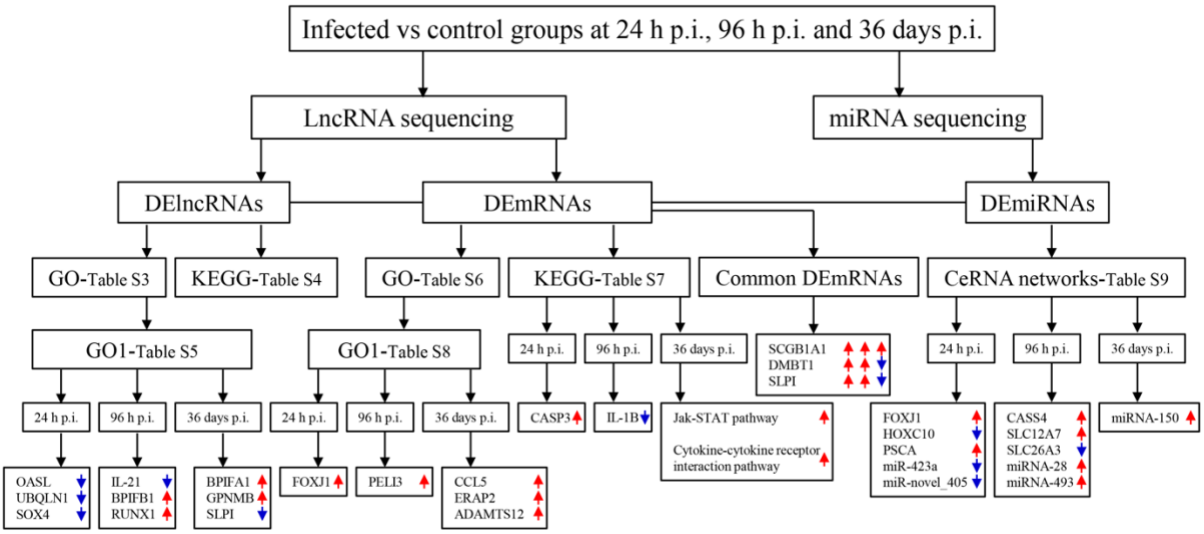
Infected vs control groups at 24 h p.i., 96 h p.i. and 36 days p.i.
LncRNA sequencing
miRNA sequencing
DElncRNAs
DEmRNAs
DEmiRNAs
GO-Table S3
KEGG-Table S4
GO-Table S6
KEGG-Table S7
Common DEmRNAs
CeRNA networks-Table S9
GO1-Table S5
GO1-Table S8
24 h p.i.
96 h p.i.
36 days p.i.
SCGB1A1
DMBT1
SLPI
OASL
UBQLN1
SOX4
IL-21
BPIFB1
RUNX1
BPIFA1
GPNMB
SLPI
FOXJ1
PELI3
CCL5
ERAP2
ADAMTS12
CASP3
IL-1B
Jak-STAT pathway
Cytokine-cytokine receptor interaction pathway
FOXJ1
HOXC10
PSCA
miR-423a
miR-novel_405
CASS4
SLC12A7
SLC26A3
miRNA-28
miRNA-493
miRNA-150

Figure 2.

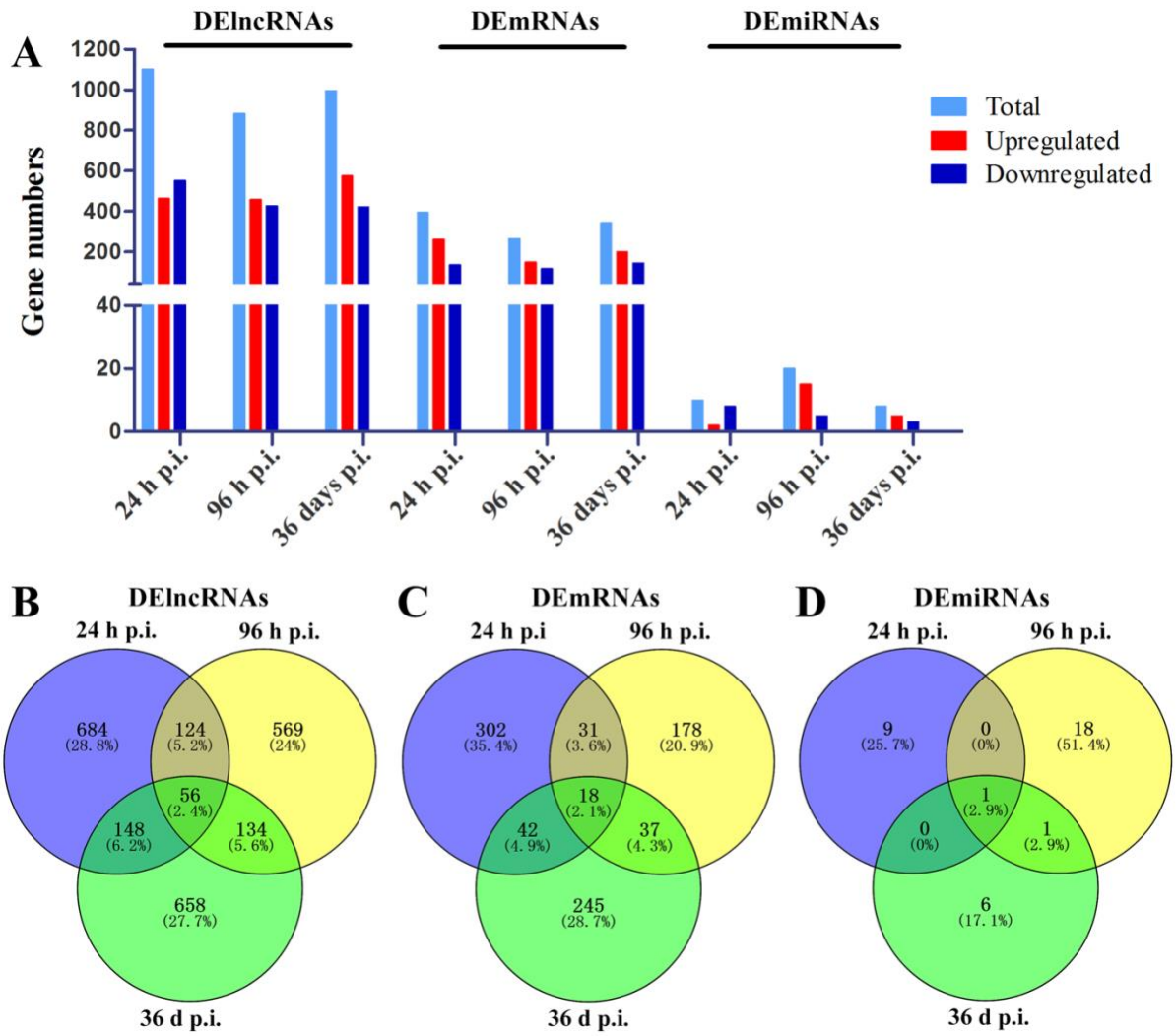
A
DElncRNAs
DEmRNAs
DEmiRNAs
Gene numbers
1200
1000
800
600
400
200
40
20
0
Total
Upregulated
Downregulated
24 h p.i.
96 h p.i.
36 days p.i.
B
DElncRNAs
24 h p.i.
96 h p.i.
684 (28. 8%)
124 (5. 2%)
569 (24%)
56 (2. 4%)
148 (6. 2%)
134 (5. 6%)
658 (27. 7%)
36 d p.i.
C
DEmRNAs
24 h p.i
96 h p.i.
302 (35. 4%)
31 (3. 6%)
178 (20. 9%)
18 (2. 1%)
42 (4. 9%)
37 (4. 3%)
245 (28. 7%)
36 d p.i.
D
DEmiRNAs
24 h p.i.
96 h p.i.
9 (25. 7%)
0 (0%)
18 (51. 4%)
1 (2. 9%)
0 (0%)
1 (2. 9%)
6 (17. 1%)
36 d p.i.

Figure 3.

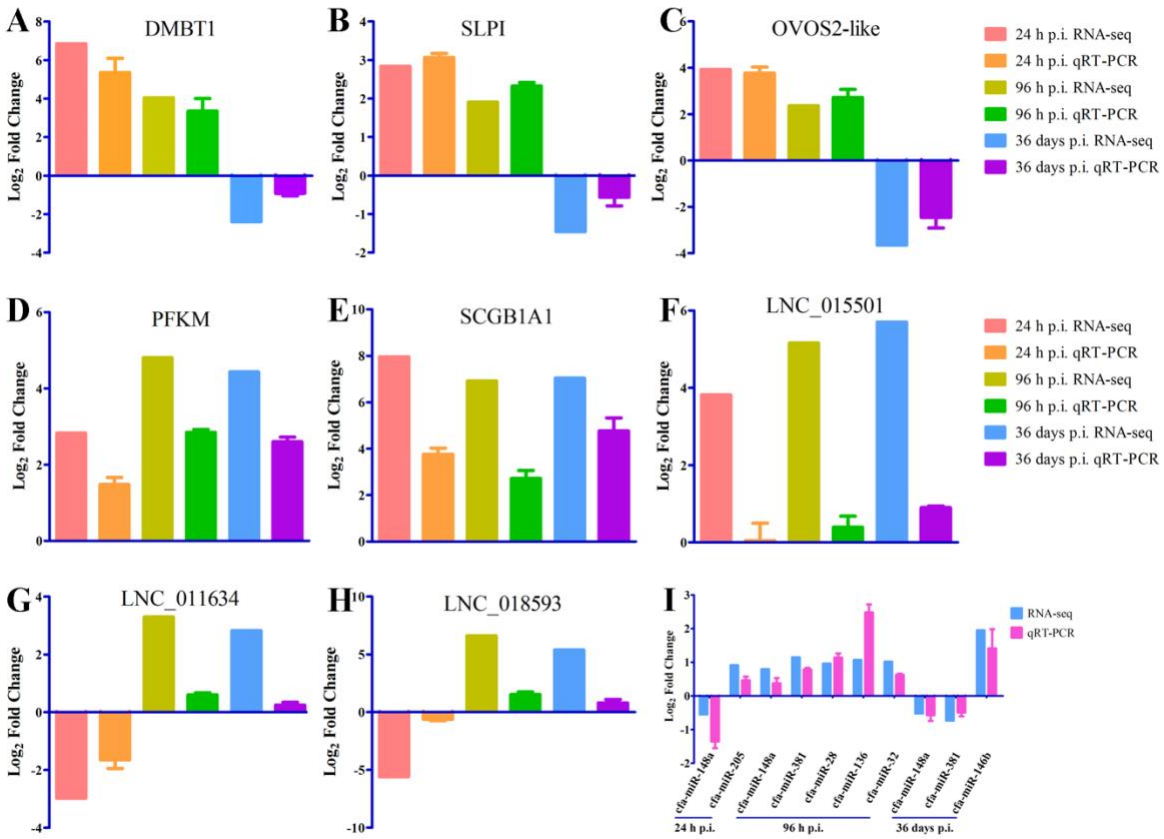
A
DMBT1
B
SLPI
C
OVOS2-like
D
PFKM
E
SCGB1A1
F
LNC_015501
G
LNC_011634
H
LNC_018593
I
Log2 Fold Change
24 h p.i. RNA-seq
24 h p.i. qRT-PCR
96 h p.i. RNA-seq
96 h p.i. qRT-PCR
36 days p.i. RNA-seq
36 days p.i. qRT-PCR
RNA-seq
qRT-PCR
cfa-miR-148a
cfa-miR-205
cfa-miR-148a
cfa-miR-381
cfa-miR-28
cfa-miR-136
cfa-miR-32
cfa-miR-148a
cfa-miR-381
cfa-miR-146b
24 h p.i.
96 h p.i.
36 days p.i.

Figure 4.

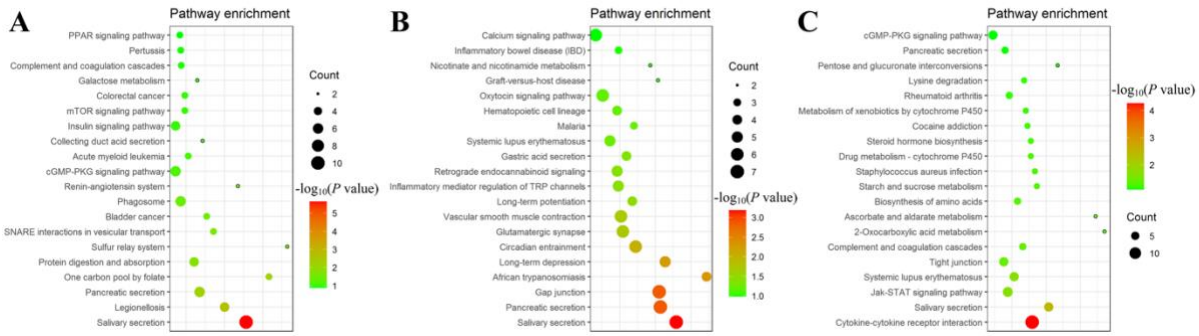
A
Pathway enrichment
PPAR signaling pathway
Pertussis
Complement and coagulation cascades
Galactose metabolism
Colorectal cancer
mTOR signaling pathway
Insulin signaling pathway
Collecting duct acid secretion
Acute myeloid leukemia
cGMP-PKG signaling pathway
Renin-angiotensin system
Phagosome
Bladder cancer
SNARE interactions in vesicular transport
Sulfur relay system
Protein digestion and absorption
One carbon pool by folate
Pancreatic secretion
Legionellosis
Salivary secretion
Count
2
4
6
8
10
-log10(P value)
5
4
3
2
1
B
Pathway enrichment
Calcium signaling pathway
Inflammatory bowel disease (IBD)
Nicotinate and nicotinamide metabolism
Graft-versus-host disease
Oxytocin signaling pathway
Hematopoietic cell lineage
Malaria
Systemic lupus erythematosus
Gastric acid secretion
Retrograde endocannabinoid signaling
Inflammatory mediator regulation of TRP channels
Long-term potentiation
Vascular smooth muscle contraction
Glutamatergic synapse
Circadian entrainment
Long-term depression
African trypanosomiasis
Gap junction
Pancreatic secretion
Salivary secretion
Count
2
3
4
5
6
7
-log10(P value)
3.0
2.5
2.0
1.5
1.0
C
Pathway enrichment
cGMP-PKG signaling pathway
Pancreatic secretion
Pentose and glucuronate interconversions
Lysine degradation
Rheumatoid arthritis
Metabolism of xenobiotics by cytochrome P450
Cocaine addiction
Steroid hormone biosynthesis
Drug metabolism - cytochrome P450
Staphylococcus aureus infection
Starch and sucrose metabolism
Biosynthesis of amino acids
Ascorbate and aldarate metabolism
2-Oxocarboxylic acid metabolism
Complement and coagulation cascades
Tight junction
Systemic lupus erythematosus
Jak-STAT signaling pathway
Salivary secretion
Cytokine-cytokine receptor interaction
-log10(P value)
4
3
2
Count
5
10

Figure 5.

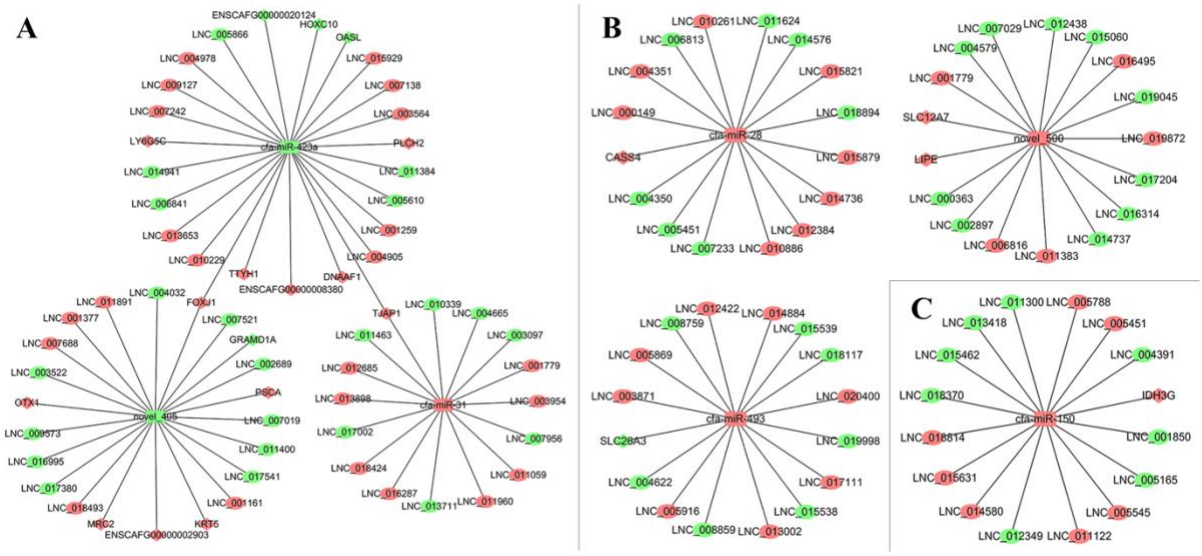
A
ENSCAFG00000020124
HOXC10
LNC_005866
OASL
LNC_004978
LNC_015929
LNC_009127
LNC_007138
LNC_007242
LNC_003564
LY6G5C
cfa-miR-423a
PLCH2
LNC_014941
LNC_011384
LNC_006841
LNC_005610
LNC_013653
LNC_001259
LNC_010229
LNC_004905
TTYH1
DNAAF1
ENSCAFG00000008380
LNC_004032
LNC_011891
FOXJ1
LNC_001377
LNC_007521
LNC_007688
GRAMD1A
LNC_003522
LNC_002689
OTX1
PSCA
novel_405
LNC_009573
LNC_007019
LNC_016995
LNC_011400
LNC_017380
LNC_017541
LNC_018493
LNC_001161
MRC2
KRT5
ENSCAFG00000002903
TJAP1
LNC_010339
LNC_004665
LNC_011463
LNC_003097
LNC_012685
LNC_001779
LNC_013898
cfa-miR-31
LNC_003954
LNC_017002
LNC_007956
LNC_018424
LNC_011059
LNC_016287
LNC_011960
LNC_013711
B
LNC_010261
LNC_011624
LNC_006813
LNC_014576
LNC_004351
LNC_015821
LNC_000149
LNC_018894
cfa-miR-28
CASS4
LNC_015879
LNC_004350
LNC_014736
LNC_005451
LNC_012384
LNC_007233
LNC_010886
LNC_012422
LNC_014884
LNC_008759
LNC_015539
LNC_005869
LNC_018117
LNC_003871
LNC_020400
cfa-miR-493
SLC26A3
LNC_019998
LNC_004622
LNC_017111
LNC_005916
LNC_015538
LNC_008859
LNC_013002
LNC_007029
LNC_012438
LNC_004579
LNC_015060
LNC_001779
LNC_016495
LNC_019045
SLC12A7
novel_590
LNC_019872
LIPE
LNC_017204
LNC_000363
LNC_016314
LNC_002897
LNC_014737
LNC_006816
LNC_011383
C
LNC_011300
LNC_005788
LNC_013418
LNC_005451
LNC_015462
LNC_004391
LNC_018370
IDH3G
cfa-miR-150
LNC_018814
LNC_001850
LNC_015631
LNC_005165
LNC_014580
LNC_005545
LNC_012349
LNC_011122

Figure 6.

Table 1

Primers used for the quantitative real-time PCR experiment in this study.

Types	Genes	Forward primers	Reverse primers
mRNA	DMBT1	CTCCAGTCCTTCCGATGATAAC	GACAACCTCAGTGTCAGGATAG
	SLPI	GCCAGTGTCTGATGCTCAAT	TTTCCCACACATGCCCTTAC
	OVOS2-like	GACACTGCTGTCTGTCTTCTT	TGACCTGGAACATCTCATTGG
	PFKM	GGAGCCCAACTCCATTTGATA	TGGCAAAGATCCTCCCATTAC
	SCGB1A1	GCAGACATGAAAGATGCAATGA	AATGAAGGGAGCTGTGTACC
lncRNA	LNC_015501	GGTTGGAACAGCCTCAATCT	CACAATCTAGGCATTGGAGGAG
	LNC_011634	CATTTCAGCAGCAGGCTTTC	CCCAGACCAGGACATATTCATC
	LNC_018593	TCAGCCTCACTCAGGTCA	CAGCCTCCATCCCAGATTAC
	L13A[a]	GCCGGAAGGTTGTAGTCGT	GGAGGAAGGCCAGGTAATTC
miRNA	cfa-miR-148a	CTGGGTCTGGTCAGTGCACTAC	
	cfa-miR-205	GGTCCTTCATTCCACCGGAGTCT	
	cfa-miR-381	CTGGTATACAAGGGCAAGCTCTCTGT	
	cfa-miR-28	GCACTAGATTGTGAGCTCCTGG	
	cfa-miR-136	CTGGGTCTGGACTCCATTTGTTTTGATGATGGA	
	cfa-miR-32	GCGGTATTGCACATTACTAAGTTGC	
	cfa-miR-146b	GCGGTGAGAACTGAATTCCATAGG	
	U6[b]	CGCTTCGGCAGCACATATAC	

[a] L13A (ribosomal protein L13A) is the house-keeping gene used for normalizing the level of mRNAs and long non-coding RNAs (lncRNAs).

[b] U6 small nuclear RNA is the house-keeping gene used for normalizing the level of microRNAs (miRNAs).

Table 2

The common signaling pathways with ⩾ 3 differentially expressed mRNAs in the lungs of Beagle dogs infected by *Toxocara canis* at 24 h p.i., 96 h p.i. and 36 days p.i.

Terms ID	Signaling pathways	Number of enriched DEmRNAs in a pathway		
		24 h p.i.	96 h p.i.	36 days p.i.
cfa01100	Metabolic pathways	18	9	18
cfa04060	Cytokine-cytokine receptor interaction	4	6	14
cfa04970	Salivary secretion	10	7	6
cfa04022	cGMP-PKG signaling pathway	6	5	6
cfa04972	Pancreatic secretion	6	7	4
cfa04020	Calcium signaling pathway	5	6	5
cfa04510	Focal adhesion	6	3	6
cfa04024	cAMP signaling pathway	3	5	6
cfa04151	PI3K-Akt signaling pathway	5	4	5
cfa05322	Systemic lupus erythematosus	3	5	6
cfa04530	Tight junction	4	4	6
cfa04010	MAPK signaling pathway	5	3	5
cfa04015	Rap1 signaling pathway	4	6	3
cfa04080	Neuroactive ligand-receptor interaction	4	3	5
cfa00230	Purine metabolism	3	4	5
cfa05034	Alcoholism	3	4	4
cfa01200	Carbon metabolism	3	3	4

Supplementary data

Supplementary data to this article can be found online at https://doi.org/10.1016/j.ijpara.2020.07.014.